CHALMERS
UNIVERSITY OF TECHNOLOGY

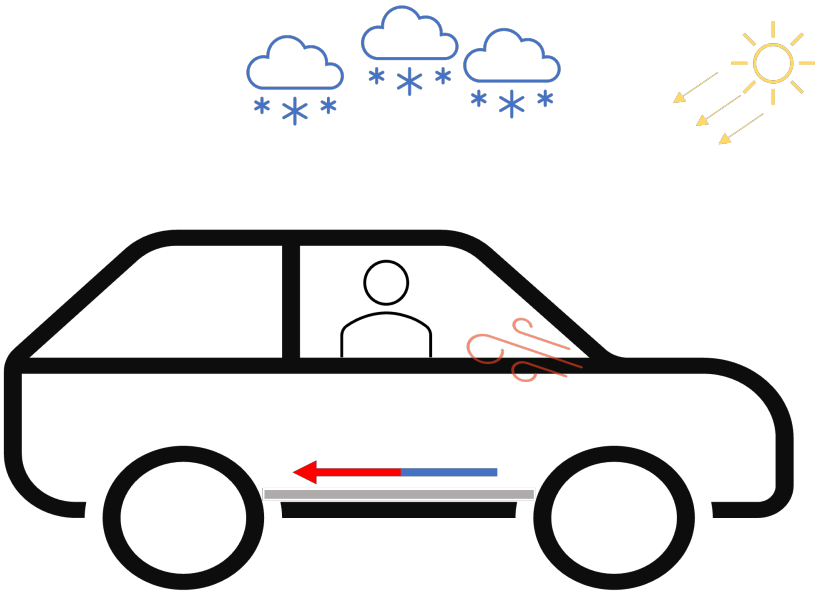

Thermal Plant Modelling of Climate System in Battery Electric Vehicles

Simulation Tool for Control Software Integration Enabling Verification of the Thermal Energy Management System

Master's thesis in Systems, Control and Mechatronics

JULIUS BENGTSSON, HANNA HALLBERG

DEPARTMENT OF ELECTRICAL ENGINEERING
CHALMERS UNIVERSITY OF TECHNOLOGY
Gothenburg, Sweden 2023
www.chalmers.se

Master's Thesis 2023

Thermal Plant Modelling of Climate System in Battery Electric Vehicles

Simulation Tool for Control Software Integration Enabling Verification of the Thermal Energy Management System

JULIUS BENGTSSON, HANNA HALLBERG

CHALMERS
UNIVERSITY OF TECHNOLOGY

DEPARTMENT OF ELECTRICAL ENGINEERING
Chalmers University of Technology
Gothenburg, Sweden 2023

Thermal Plant Modelling of Climate System in Battery Electric Vehicles
Simulation Tool for Control Software Integration Enabling Verification of the Thermal Energy Management System
JULIUS BENGTSSON, HANNA HALLBERG

Supervisor: Mikael Larsson, CEVT AB
Examiner: Jonas Sjöberg, Department of Electrical Engineering

Master's Thesis 2023
DEPARTMENT OF ELECTRICAL ENGINEERING
Chalmers University of Technology
SE-412 96 Gothenburg
Sweden
Telephone +46 31 772 1000

Cover: Illustration of a car with different ambient conditions and thermal management acting on battery and cabin.

Typeset in LaTeXusing a template created by Magnus Gustaver
Gothenburg, Sweden 2023

Thermal Plant Modelling of Climate System in Battery Electric Vehicles
Simulation Tool for Control Software Integration Enabling Verification of the Thermal Energy Management System
JULIUS BENGTSSON, HANNA HALLBERG
Department of Electrical Engineering
Chalmers University of Technology

Abstract

An efficient thermal energy management (TEM) system is crucial to extend the driving range of battery electric vehicles (BEV). To evaluate its performance during development, a time-efficient simulation tool is needed. At China Euro Vehicle Technology AB (CEVT), the developed TEM software is tested using GT-SUITE simulations. It is a very accurate simulation tool, but computationally heavy and time-consuming with an execution time in the magnitude of days. Therefore, CEVT has developed an analytical plant model of the TEM system for a specific ambient temperature. This model is however limited to one ambient temperature and not compatible with measurement data collected from their physical car. Therefore, a generalized mathematical plant model of the thermal system in BEVs has been developed in this work, which captures the TEM system's behavior at a larger ambient temperature range.

The components in the proposed model are designed individually, such that the refrigerant and coolant circuit can be tested separately in addition to the performance of the complete TEM model. Inputs to the plant model are explicitly control signals enabling the model to function independently of unavailable measurements from the vehicle. Therefore, the pressure difference in the refrigerant circuit must be determined using control signals. The pressure difference over the two expansion valves is modeled using a modified version of the Bernoulli equation for a single short orifice valve.

Simulation results show that the proposed model represents the system with its dynamic behavior. The model captures changes in the input signals qualitatively well, although the exact numerical values often are a bit off, but the model finds a new stable equilibrium point to operate at. All verified temperatures show model outputs in an acceptable RMS error range, indicating the model accomplishes the aim of being general.

Keywords: BEV, Climate system, Heat pump, HVAC, Simulation, System modeling, TEM.

Acknowledgements

We would like to thank the employees at CEVT for giving us the opportunity to perform this thesis and for their great hospitality. Especially we would like to thank our supervisor Mikael Larsson at CEVT for his engagement and interesting ideas during the project. We would also like to express our gratitude to our examiner Jonas Sjöberg at Chalmers University of Technology who has guided us throughout the project.

Julius Bengtsson & Hanna Hallberg, Gothenburg, May 2023

List of Acronyms

Below is the list of acronyms that have been used throughout this thesis listed in alphabetical order:

ACC	Air Cooled Condenser
BEV	Battery Electric Vehicle
CEVT	China Euro Vehicle Technology
CTEM	CEVT Thermal Energy Management
EXV	Electronic Expansion Valve
HVAC	Heat, ventilation, and air conditioning
NTU	Number of Transfer Units
RMSE	Root Mean Square Error
RPM	Revolutions Per Minute
SoC	State of Charge
TEM	Thermal Energy Management
WCC	Water Cooled Condenser
WLTP	Worldwide Harmonised Light Vehicle Test Procedure

Nomenclature

Below is the nomenclature of parameters and variables that have been used throughout this thesis.

Parameters

$\epsilon_{\text{accPhaseShift}}$	Air cooled condenser effectiveness
ϵ_{batt}	Battery effectiveness
$\epsilon_{\text{chillPhaseShift}}$	Chiller effectiveness
ϵ_{em}	Electric motor effectiveness
$\epsilon_{\text{evapPhaseShift}}$	Evaporator effectiveness
$\epsilon_{\text{radCross}}$	Radiator effectiveness
$\epsilon_{\text{wccCross}}$	Water cooled condenser effectiveness
ω	Compressor speed
$\dot{\omega}$	Compressor acceleration
b_{cold}	Waste cold air
b_{hot}	Waste hot air
C_{c}	Heat capacity rate corresponding to the cold stream
C_{h}	Heat capacity rate corresponding to the hot stream
C_{min}	Smallest heat capacity rate
h_{acc}	Specific enthalpy of the refrigerant at air cooled condenser outlet
$h_{\text{chillRefOut}}$	Specific enthalpy of the refrigerant at the chiller outlet
$h_{\text{chillVapor}}$	Specific enthalpy to vaporize in the chiller
$h_{\text{evapRefOut}}$	Specific enthalpy of the refrigerant at the evaporator outlet
$h_{\text{evapVapor}}$	Specific enthalpy to vaporize in the evaporator
$\dot{\text{m}}_{\text{evapAir}}$	Air mass flow rate over evaporator
$\dot{\text{m}}_{\text{accAir}}$	Air mass flow rate over condenser
$\dot{\text{m}}_{\text{edClnt}}$	Coolant mass flow rate in electric drive

$\dot{m}_{\text{wccClnt}}$	Coolant mass flow rate over water cooled condenser
$\dot{m}_{\text{radAir}}$	Air mass flow rate over radiator
$\dot{m}_{\text{cmpr}}$	Refrigerant mass flow rate at compressor outlet
$\dot{m}_{\text{chillRef}}$	Refrigerant mass flow rate over chiller
$\dot{m}_{\text{chillClnt}}$	Coolant mass flow rate over chiller
$\dot{m}_{\text{evapRef}}$	Refrigerant mass flow rate over evaporator
$\dot{m}_{\text{HVAC}}$	Air mass flow rate into cabin
P_{s}	Suction pressure
$P_{\text{s,new}}$	Updated suction pressure
P_{d}	Discharge pressure
$P_{\text{d,new}}$	Updated discharge pressure
ΔP	Pressure difference over compressor
$\dot{Q}_{\text{em}}$	Heat transfer rate between em and coolant
$\dot{Q}_{\text{wcc}}$	Heat transfer rate in water cooled condenser
$\dot{Q}_{\text{rad}}$	Heat transfer rate in radiator
$\dot{Q}_{\text{generative}}$	Heat transfer rate generated in battery
$\dot{Q}_{\text{cool}}$	Heat transfer rate between coolant and battery
$\dot{Q}_{\text{evapVapor}}$	Heat transfer rate in evaporator changing phase
$\dot{Q}_{\text{evapTemp}}$	Heat transfer rate in evaporator changing temperature
$\dot{Q}_{\text{chillVapor}}$	Heat transfer rate in chiller changing phase
$\dot{Q}_{\text{chillerTemp}}$	Heat transfer rate in chiller changing temperature
$\dot{Q}_{\text{accCond}}$	Heat transfer rate in air cooled condenser changing phase
$\dot{Q}_{\text{accTemp}}$	Heat transfer rate in air cooled condenser changing temperature
$\dot{Q}_{\text{HVAC}}$	Heat transfer rate between providing hot/cold air
$\dot{Q}_{\text{pass}}$	Heat transfer rate caused passenger
T_{c}	Critical temperature
T_{sub}	Subcooling temperature
$T_{\text{h,in}}$	Inlet temperature of hot stream
$T_{\text{c,in}}$	Inlet temperature of cold stream
T_{batt}	Battery temperature
$T_{\text{battClntIn}}$	Coolant temperature battery inlet
$T_{\text{battClntOut}}$	Coolant temperature battery outlet
T_{cabin}	Cabin air temperature
$T_{\text{chillClntIn}}$	Coolant temperature chiller inlet

$T_{\text{chillClntOut}}$	Coolant temperature chiller outlet
$T_{\text{chillRefOut}}$	Refrigerant temperature chiller outlet
T_{em}	EM temperature
T_{emClntIn}	Coolant temperature em inlet
$T_{\text{emClntOut}}$	Coolant temperature em outlet
T_{cmprOut}	Temperature compressor outlet
$T_{\text{radClntOut}}$	Coolant temperature radiator outlet
$T_{\text{radClntIn}}$	Coolant temperature radiator inlet
$T_{\text{wccClntOut}}$	Coolant temperature WCC outlet
$T_{\text{wccRefOut}}$	Refrigerant temperature WCC outlet
$T_{\text{accAirOut}}$	Air temperature ACC outlet
$T_{\text{accRefOut}}$	Refrigerant temperature ACC outlet
$T_{\text{ambientAir}}$	Ambient air temperature
$T_{\text{evapAirIn}}$	Air temperature evaporator inlet
$T_{\text{evapAirOut}}$	Air temperature evaporator outlet
$T_{\text{evapRefOut}}$	Refrigerant temperature evaporator outlet
T_{exvOut}	Refrigerant temperature exv outlet
T_{s}	Refrigerant suction temperature
T_{d}	Refrigerant discharge temperature
T_{HVAC}	Air temperature provided to cabin
T_{cabinAir}	Air temperature in cabin
U	Heat transfer coefficient
v	Vehicle velocity
z_{evap}	Expansion valve position into evaporator
$\dot{z}_{\text{evap}}$	Rate of expansion valve position into evaporator
z_{chill}	Expansion valve position into chiller
$\dot{z}_{\text{chill}}$	Rate of expansion valve position into chiller

Variables

ρ_{s}	Density compressor inlet
a_0, a_1, a_2, a_3, a_4	Expansion valve coefficients
A	Total flow area expansion valve
$c_{\text{p,air}}$	Specific heat capacity of air

$c_{\mathrm{p,batt}}$	Specific heat capacity of the battery
$c_{\mathrm{p,clnt}}$	Specific heat capacity of coolant
$c_{\mathrm{p,ref}}$	Specific heat capacity of refrigerant
C_D	Mass flow coefficient
d_{chill}	Flow area expansion valve into chiller
d_{evap}	Flow area expansion valve into evaporator
D	Throat area expansion valve
I_{batt}	Battery current
$k_{\mathrm{evap}}, k_{\mathrm{chill}}, k_{\mathrm{acc}}$	NTU correction factor
k_{z}	Expansion valve position constant
k_{ω}	Compressor speed constant
q_{qual}	Quality line
R_{bus}	Bus bar resistance in the battery
R_{int}	Internal battery resistance
V_{cabin}	Volume passenger cabin
x_1, x_2	Model fitting parameters

Contents

List of Figures

List of Tables

1

Introduction

This chapter presents the challenges battery electric vehicles (BEV) are facing and the importance of an efficient thermal system. Further how a simulation model can be utilized to improve software development along with the contribution of related and previous research.

The automotive industry is experiencing one of the largest transformations in its history. The shift from fossil fuels towards electric power is imposed by sustainability and economic drivers. It is estimated that 30% of the worldwide sales of passenger vehicles in 2032 will be BEVs [1]. One main concern towards BEVs is the driving range which is affected by all loads, such as the load from the electric motors but also supports systems for the driver and comfort for the passengers. One of the largest factors that affect the range is the climate in which the vehicle operates. In extreme conditions the range can be reduced by over 50% [2].

Combustion engines generate excess heat which electric motors do not do to the same extent. With the system no longer having an overflow of energy in combination with components, such as the battery, with a strict operating window, an efficient thermal system is required. The system needs to keep the temperature of the battery in the correct range, provide a comfortable temperature in the passenger cabin, and at the same time not consume too much power. The complexity of the thermal energy management (TEM) system has grown and efficiently transferring heat from one component to apply it at a different part of the thermal system is essential to increase driving range.

A cost-effective way to extend the driving range is by increasing the efficiency of the TEM system. Therefore a time-efficient simulation tool of the thermal system in BEVs is needed, to be able to quickly test software updates. The thermal system dynamics in electric cars at the China Euro Vehicle Technology AB (CEVT) are currently tested using GT-SUITE. This simulation tool enables verification of the developed software using a very accurate 1-D plant model. The simulations are however computationally heavy and time-consuming. The battery is for instance modeled as individual cells leading to a plant model with a large amount of data points. Running simulations in GT-SUITE therefore executes in a magnitude of days, introducing the need for a time-efficient tool to simulate the thermal system.

1.1 Related work

As the simulations in GT-SUITE are time-consuming and computationally heavy an analytical plant model of the TEM system was developed by a PhD student for CEVT [3]. It is a mathematical model of the thermal system used in CEVT's cars developed for a specific cool-down case with an ambient temperature of 45°C. The approach used optimization parameters to adapt the model to measurements generated from GT-SUITE, which proved high accuracy in estimated simulation outputs and power consumption. Where the simulation only takes a few seconds to execute, compared with the run time in GT-SUITE. Moreover, the control signals and model outputs used to validate and optimize the model are GT-SUITE data generated from one Worldwide Harmonised Light Vehicle Test Procedure (WLTP) driving cycle, see Section 2.1.2. An issue with using optimization variables is that the model characteristic is dependent on the file of reference such that the model output for a different use case is not reliable. The model has a small error for the specific WLTP test cycle but has difficulties representing the system behavior in other ambient conditions. The simulation data collected from GT-SUITE is also with the car in a steady state. This means that the battery, cabin, and thermal system initially is at the desired temperature.

1.2 Contribution

This project aims to develop a generalized mathematical plant model of the thermal system in BEVs. A proposed mathematical model to capture the behavior of the physical car such that it can be used as a tool to quickly test and verify software changes. It is important that the model manages to represent the system at different ambient temperatures and user scenarios rather than being very accurate for a specific use case. Therefore it is verified on four different ambient temperatures, that is -10°C, 0°C, 40°C, and 45°C.

In contrast to control signals and model outputs generated from simulations in GT-SUITE, this project utilized measurement files from a prototype vehicle, described in Section 2.1.1, to design a generalized plant model. The designed model run on physical data described in Section 2.1.2, such that the simulated output represents the expected behavior of the physical product.

In addition to the existing model, all cooling modes in the coolant circuit are represented in the developed plant model. As the climate the car operates in varies, the cooling need in the TEM system changes. Different cooling modes enable the system to either actively or passively cool the components, which is further described in Section 2.1. A model of the electric drive (ED) circuit was developed to complete the modelling of all cooling modes. Moreover, the existing model utilizes pressure measurements whereas the input to the developed model are control signals. The model, therefore, estimates the pressure difference over the expansion valves as described in Section 2.2.2 and is not dependent on measurements. The developed model is independent and operates as a simulation tool with only control signals as input.

1.3 Limitations

The plant model is tested for four ambient temperatures, that is $-10°$, $0°$, $40°$, and $45°$. The WLTP drive cycle described in section 2.1.2 is used for validation and the model is not evaluated against other driving patterns or a larger temperature range. The plant model supports all 4 modes in the CTEM, with one not validated due to unavailable measurements.

Like the plant model presented in Section 1.1 the measurements used are with the prototype vehicle at steady state. If the car is not in a steady state it is possible that the system changes mode within a driving cycle as the cooling needs changes. A behavior the model is not validated for. The input to the plant model is control signals collected from the WLTP drive. It means that the controller does not act on feedback from the model outputs. Instead, the control signals, which are inputs to the plant model, are predetermined by the measurement file.

1.4 Thesis outline

The initial Chapter 2 introduces the theory with concepts and terminology utilized in the modeling being explained to prepare the reader for the later chapters. The heating, ventilation, and air conditioning (HVAC) system has a central role in a TEM system to enable efficient heat transfer and is explained in Section 2.2. Chapter 3 applies the theory to design a model of the CTEM with the system being divided into two subsystems, the coolant circuit in Section 3.2 and the refrigerant circuit in Section 3.3. These two subsystems are coupled together to form the complete system together with a model of the cabin. This chapter describes how the model is implemented with the relation of the subsystems explained with a mathematical model and the two subsystems are assessed individually. The complete model is then evaluated in Chapter 4. The presented results and their findings are discussed in Chapter 5. Finally, Chapter 6 highlights areas where the model can be further developed to extend its usage and benefits in the future.

2
Theory

This chapter includes the theory of how the thermal energy system is designed to work with an explanation of its individual components. The system is split into two subsystems, the refrigerant and coolant circuit, with its properties described and how energy can be transferred between the closed circuits and altered to minimize the consumed energy. Lastly, the adjustments in the model are listed to account for uncertainties.

2.1 Thermal energy management system overview

A TEM system controls not only the user-experienced cabin temperature but also the complete drivetrain to ensure the battery and the electric motors operate efficiently at a stable temperature. For BEVs, an efficient system is a necessity to produce a competitive car. All energy consumed by nonessential systems, with parts of the thermal system being one of them, reduces the driving range which is a key aspect to optimize. The excessive heat created by a combustion engine is more than the system consumes, BEVs have to spend energy to create this heat which is produced with a heat pump system. The system can produce the requested amount of heat without waste to lower energy usage. There are ways to reduce the energy consumed to run the heat pump, as other parts of the system have losses in the form of heat when operating that can be utilized and preserved within the system.

An overview of the CTEM can be seen in Figure 2.1 with three separated circuits illustrated. The system can be divided into two subsystems with the two coolant circuits being one and the refrigerant being the second. The circuit marked in green is the refrigerant one which is explained in Section 2.2. The coolant subsystem is controlled by valves which allow it to alter between different modes to match the required cooling need for varying ambient conditions. The subsystems are connected at two points allowing heat to be exchanged between the two. The chiller transfers heat from the coolant to the cold refrigerant while that exchange in the water-cooled condenser (WCC) is from the warm refrigerant to the coolant. With heat being transferred from one subsystem to the other, energy is preserved and utilized in a different part of the system. The coolant system also has a radiator that can remove additional heat from the system in order of maintaining a desired temperature, with energy being dumped from the system to the ambient air.

The battery needs a specific range of operating temperature which requires cooling in warm conditions to counter the developed heat. In contrast at cold conditions, the battery requires heating to reach an optimal operating point. The electric motor

develops heat when active, the motor has a high efficiency but as the system recovers its generated heat, the energy is preserved within the system. The yellow circuit in Figure 2.1 has a valve after the pump that controls the flow over the electric motor and how much heat can be recovered over the WCC.

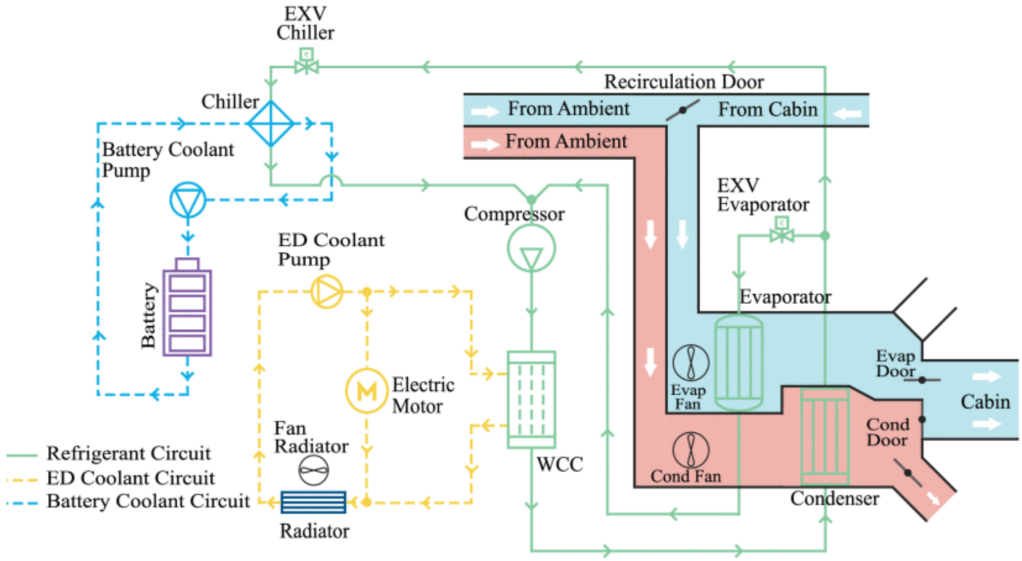

Figure 2.1: Schematic overview of the CTEM system used at CEVT

In addition to the refrigerant and coolant circuits, the air is utilized to remove but also generate heat into the system. Ambient air blows over the radiator to remove excess heat and reduce the temperature of the coolant liquid. Air entering the cabin flows in one of the two channels colored red and blue in Figure 2.1. Ambient air flowing over the ACC absorbs heat from the warmer refrigerant gas. The other intake combines air from the cabin with ambient air with the ratio decided by the recirculation door. The mixed air flows over the evaporator where heat is transferred to the colder refrigerant. In warm conditions, recirculating cabin air is energy efficient as it requires less cooling. Depending on the conditions and what the AC request, the two air flows are controlled by doors to get the correct air mix flowing into the cabin.

2.1.1 Test vehicle

The CTEM system developed by CEVT is used by Zeekr in cooperation with the autonomous vehicle company Waymo, with the vehicle illustrated in Figure 2.2. The vehicle is a project under the development phase with only prototype vehicles being built and is not yet on the market. The vehicle is used to collect measurements from driving cycles. The data is utilized to verify the simulation model behavior with the vehicle as a reference.

Figure 2.2: Waymo vehicle with CTEM system, [Source: Waymo]

2.1.2 Driving cycle

The WLTP is a test procedure aimed to provide reference measurements that are comparable worldwide [4]. It provides a standard for determining the CO_2 emissions, level of pollutants and fuel consumption, or driving range of electric vehicles. The WLTP test procedure is divided into four parts, as illustrated in Figure 2.3, with different average speeds representing the everyday driving profile. Each part also contains different driving phases, such as stops, acceleration, and braking.

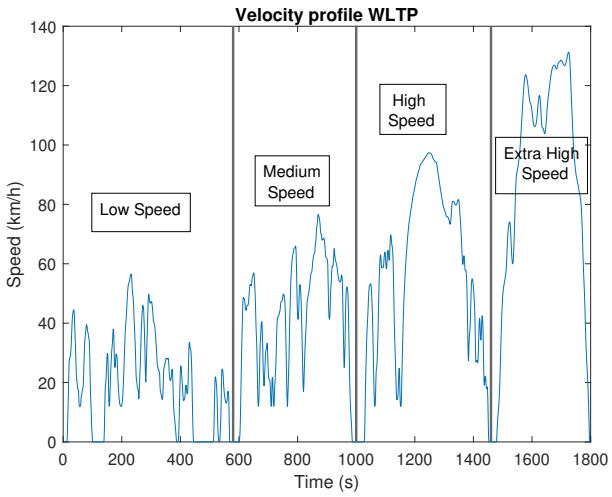

Figure 2.3: Scheduled speed profile of the vehicle in a WLTP driving cycle

The input and output signals used to verify the plant model are collected from the

drive cycles of the WLTP test sequence. The prototype car has been tested against the WLTP profile for different ambient temperatures and initial conditions. Where the measurement data used to validate the model are with the vehicle in a steady state. It means that the passenger cabin and battery are preheated in cold ambient conditions, and cooled in warmer. The speed profile of the test sequence is required to calculate the power consumption of the electric motor. A standardized test cycle like the WLTP is selected to have comparable data and a repeatable sequence.

2.2 Heating, ventilation, and air conditioning

The refrigerant circuit is a HVAC system with a heat pump that operates on the vapor-compressor cycle. It consists of a high pressure side and a low pressure side as shown in Figure 2.4. The compressor is used to maintain the low pressure side and control the refrigerant flow of the system [5]. By compressing the gas it increases the pressure of the refrigerant vapor from the evaporators such that it later in the cycle condenses. The two components in the system which utilize the evaporation process are the evaporator and chiller. In the evaporator, the refrigerant absorbs heat from the air whereas heat is removed from the coolant in the chiller. The superheated vapor leaving the compressor enters the two components which condense the refrigerant. In the WCC the refrigerant exchange heat with the coolant while the ACC uses ambient air to provide hot air. The warm air is either used to achieve a comfortable cabin temperature or dumped as waste if necessary. The refrigerant system also consists of two parallel electronic expansion valves (EXV). It is used to expand the subcooled liquid and attain a low pressure mixture of gas and liquid, which then enters the evaporators.

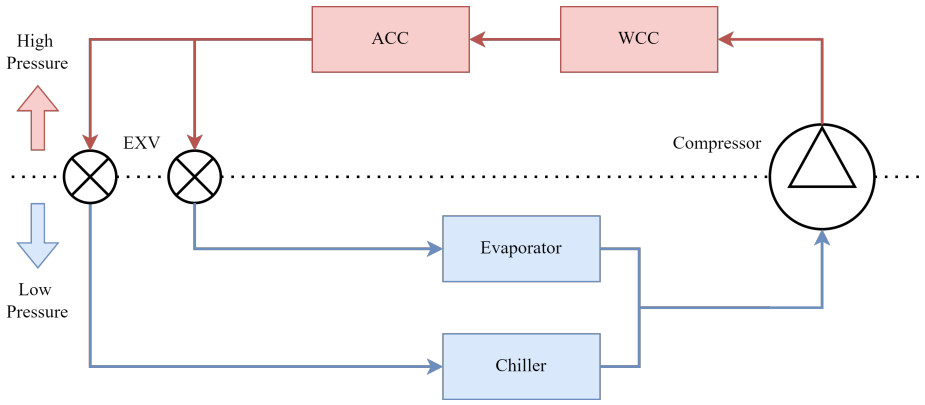

Figure 2.4: A illustration of the components in the vapor-compression cycle used in the CTEM system.

2.2.1 Vapor-compression cycle

A vapor-compression system is a refrigeration system used to transfer heat by letting the refrigerant absorb and expel heat from its surroundings [5]. Four thermal processes take place in a basic vapor-compression system and are shown in Figure 2.5, namely evaporation, compression, condensation, and expansion. This process

can be illustrated in a pressure-enthalpy diagram. The log(P)-h diagram can be divided into three parts and are separated by the saturation line for liquid and vapor respectively. The refrigerant is subcooled liquid in the leftmost region, a mixture of liquid and gas in the middle and the rightmost region is superheated vapor.

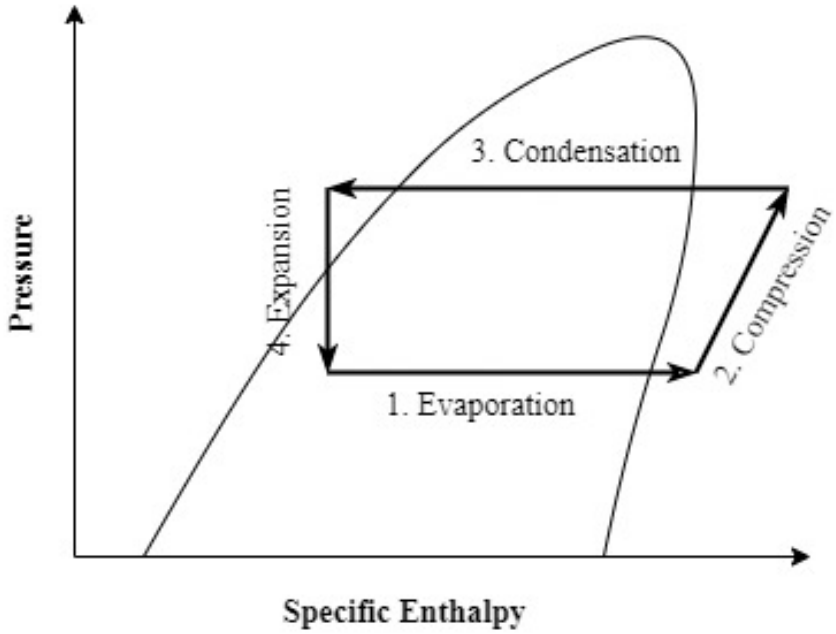

Figure 2.5: log(P)-h diagram of a basic vapor-compression cycle

2.2.1.1 Evaporation

Low pressure refrigerant mixture enters the evaporator where it vaporizes by absorbing heat [6]. Either from the ambient air from the outside or by recirculating the air in the cabin. The refrigerant leaves the evaporator as superheated gas and the air is cooled down and blown into the cabin, proving a cooling effect. The refrigerant absorbs heat at constant pressure and temperature in the mixture region, which means that the heat exchanged between the mediums is used to turn liquid into gas.

The evaporator used in the thermal system in BEVs is often called direct expansion coils [6]. It consists of a series of tubes which the refrigerant flows through. The refrigerant then absorbs heat from the air blown across the evaporator. It enters the evaporator as a low pressure mixture and leaves as a superheated gas. The amount of superheat at the coil outlet is regulated by the expansion valve.

2.2.1.2 Compression

The compressor is the driving force of the vapor-compression cycle and is the device that requires work [5]. By regulating the compressor speed the mass flow rate of the refrigerant is affected and thereby the cooling capacity of the system. The superheated vapor from the evaporator is pumped through the system to obtain the desired temperature and pressure. Another function of the compressor is to increase

the pressure of the vapor obtained in the evaporator. Due to the change in pressure, the refrigerant flows through the system.

The superheated vapor obtained from the evaporator enters the compressor at low pressure, low temperature and is compressed into a smaller volume to create a high pressure, high temperature vapor. Increasing the pressure of the gaseous refrigerant raises its boiling and condensing temperature. When it is sufficiently compressed it yields a higher boiling temperature than the surrounding mediums. Hence, the refrigerant vapor can remove its heat.

Many different types of compressors depending on use case are available, but the one used in the studied CTEM system is a scroll compressor. It uses one stationary scroll and one orbiting scroll to compress the vapor [6]. The upper scroll, which is fixed, contains the outlet of the high pressure vapor. The lower scroll on the other hand is driven by a motor which makes it orbit about the center, which is illustrated in Figure 2.6. The orbiting motion forces the refrigerant toward the center of the fixed scroll. After three orbits the compressed vapor leaves the compressor via the discharge port.

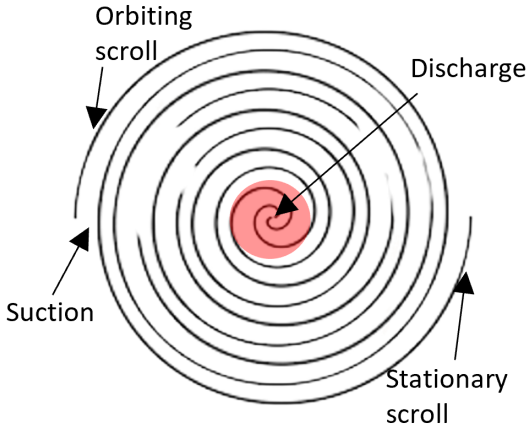

Figure 2.6: Illustration of a scroll compressor.

2.2.1.3 Condensation

Condensation is the process of changing a superheated vapor, obtained in the compressor, to a subcooled liquid. The process of condensation can be divided into three stages. Firstly de-superheating of the gas, where the gas temperature reduces to the saturation threshold. Next the refrigerant goes from gas to liquid, called the condensation stage. Lastly, the refrigerant is subcooled with the temperature reduced below the saturation point of the liquid phase. In contrast to the evaporator, it is used to excel heat and not absorb it. The high pressure refrigerant vapor can exchange heat with a coolant in a WCC or with air in an air cooled condenser (ACC). The latter is used to increase the temperature of ambient air which then is used to warm the vehicle's cabin. In a WCC the refrigerant instead excels heat to the coolant circuit. The refrigerant maintains the high pressure during the condensation but changes phase into a liquid.

The process of heat exchange between the coolant and refrigerant in a WCC is illustrated in Figure 2.7. The refrigerant flow through the shell and the coolant flow through the tubes and absorb heat [6]. An ACC work similarly, but the cooling medium is ambient air.

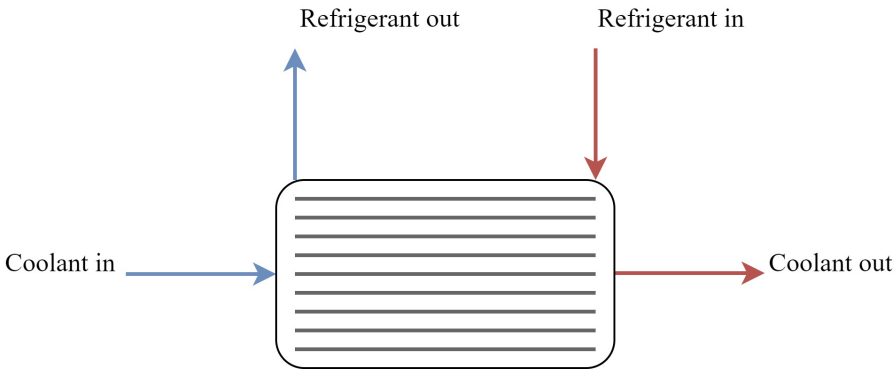

Figure 2.7: Illustration of a water cooled condenser.

2.2.1.4 Expansion

In order to reduce the pressure and temperature of the subcooled refrigerant obtained in the condenser an expansion process is sufficient. An EXV does so by adjusting the geometric throat area, which limits the flow area and therefore the refrigerant expand and the pressure is reduced [7]. Hence, the pressure and temperature at the EXV outlet are reduced. An illustration of the needle's impact on the flow area is depicted in Figure 2.8. The flow area of refrigerant is controlled by the needle's position in the orifice [8]. The flow area is the region of the total orifice area, denoted D, which is not limited by the needle with area d. In other words, the refrigerant will flow around the needle, as illustrated in the figure.

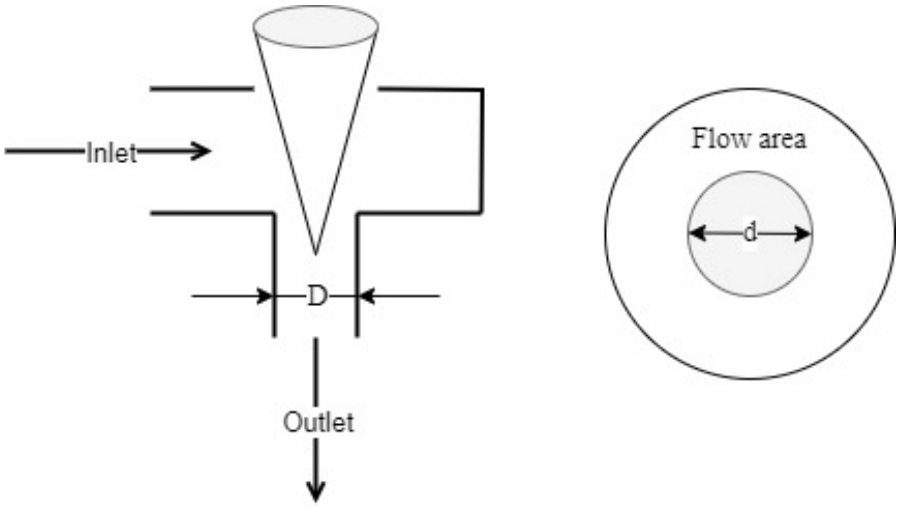

Figure 2.8: Illustration of the flow area in EXV depending on the needle's position in the throat.

Furthermore, the amount of refrigerant also affects the ability to absorb heat from the surrounding medium in the evaporator. The EXV regulates the valve position to maintain the correct amount of superheated refrigerant leaving the evaporator. It is necessary that all the refrigerant leaving the evaporator is gaseous, otherwise, the compressor can be damaged. Lastly, the expansion is the last process in the vapor-compression cycle where the condensed refrigerant liquid then is the starting point of the next cycle.

The expansion process through an EXV is an isenthalpic process. The enthalpy of the refrigerant is unchanged during the process. This means that the enthalpy of the subcooled refrigerant leaving the condenser and the refrigerant mixture leaving the EXV is assumed to be equal.

2.2.2 Pressure difference over expansion valve

The vapor-compression system is divided into a high pressure side and a low pressure side. The difference between the discharge pressure and suction pressure is estimated in each iteration. It is used to compute the discharge temperature of the compressor but is also needed in the next iteration to determine the refrigerant mass flow rate. A commonly used estimation of the mass flow rate in EXV is an equation derived from Bernoulli's equation for short orifice valves [9]. The modified equation introduces a mass flow coefficient as the flow through an EXV has shown to be mainly influenced by the valve position and the subcooling value. The equation is expressed as

$$\dot{m} = C_{\mathrm{D}} A \sqrt{2\rho_{\mathrm{s}}(P_{\mathrm{d}} - P_{\mathrm{s}})} \tag{2.1}$$

where $\dot{m}$ is the mass flow rate, C_{D} the mass flow coefficient, A the geometric throat area, ρ_{s} the density of the refrigerant at the compressor inlet, P_{d} and P_{s} is the discharged and suction pressure respectively. However, the literature predicts the mass flow rate of a single EXV whereas the CTEM system has two parallel valves. The refrigerant from the ACC outlet is divided over the evaporator and chiller requiring two valves. Therefore the throat area A is modified and is the total opening area of both the chiller and evaporator.
The result discussed in literature [9] shows that the mass flow rate in EXV is dominantly influenced by the valve position and degree of subcooling. In order to predict the mass flow rate at different conditions a correlation for the mass flow coefficient must be established. It can either be obtained using Buckingham π theorem or generated using polynomial fit. Where the latter is used to establish the correlation between the valve opening and the subcooling. The polynomial correlation can be formulated as

$$C_{\mathrm{D}} = a_0 + a_1 \cdot z + a_2 \cdot z^2 + a_3 \cdot z \cdot \frac{T_{\mathrm{sub}}}{T_{\mathrm{c}}} + a_4 \cdot \frac{T_{\mathrm{sub}}}{T_{\mathrm{c}}} \tag{2.2}$$

where $a_0, ..., a_4$ is the constants with the best fit, z is the sum of the valve opening of the two EXV, T_{sub} is the subcooling temperature and T_{c} the critical temperature. With the mass flow coefficient generated for each coolant mode, the pressure differ-

ence over the valves can be formulated as

$$(P_{\mathrm{d}} - P_{\mathrm{s}}) = \frac{\left(\frac{\dot{\mathrm{m}}}{C_{\mathrm{D}} A}\right)^2}{2\rho_{\mathrm{s}}} \tag{2.3}$$

2.3 Effectiveness-NTU method

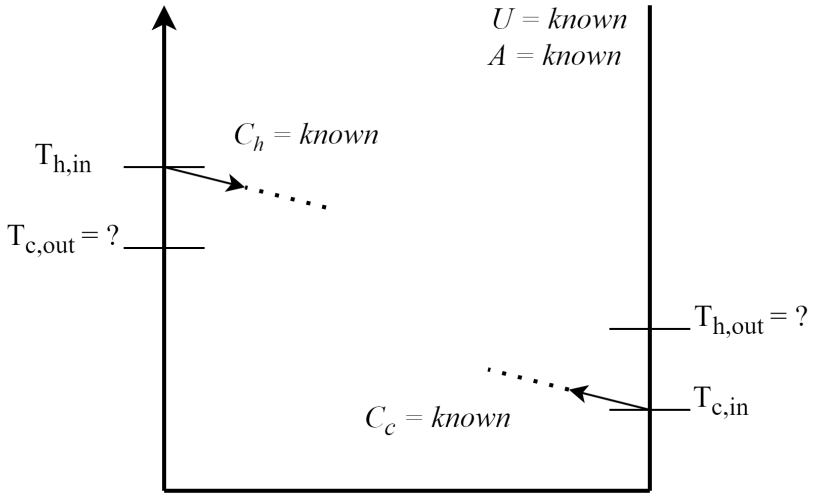

Figure 2.9: Problem description where the effectiveness-NTU method can be utilizable.

The heat rate transferred between the heat exchangers in the system and the streams is defined by its mass flow rate, specific heat capacity, and the temperature difference between the inlet and outlet temperature of the fluid [10]. The outlet temperature is however not known beforehand, nor is it an input to the plant model. Therefore the number of transfer units (NTU) method is utilized to determine the heat transfer rate and furthermore the outlet temperature. The effectiveness-NTU method is used under the assumption that the overall heat transfer coefficient in the heat exchangers is fairly uniform [11]. This is likely as the heat exchangers in the system are rather compact.

An illustration of the problem where the effectiveness-NTU method is suitable is depicted in Figure 2.9. The inlet temperature is known for both the cold and hot medium and is denoted $T_{\mathrm{c,in}}$ and $T_{\mathrm{h,in}}$ respectively. The outlet temperatures however are to be calculated using the known heat capacity rates C_{c} and C_{h}, the overall heat transfer coefficient denoted U, and the heat transfer area. The heat transfer rate is then calculated as

$$\dot{Q} = \epsilon C_{\min}(T_{\mathrm{h,in}} - T_{\mathrm{c,in}}) \tag{2.4}$$

where ϵ is a quantity between 0 and 1 which determined the heat exchanger's effectiveness. It is defined as

$$\epsilon = \frac{\text{actual heat transferred}}{\text{maximum possible heat transferred between the streams}} \tag{2.5}$$

Moreover, $C_{\min}$ is the smallest heat capacity rate of C_{c} and C_{h}.

The effectiveness-NTU method is used to determine the outlet temperatures from the evaporator and ACC in the refrigerant circuit, the heat exchange over the radiator in the coolant circuit, and over the WCC and chiller which transfer heat between the two circuits. Firstly $C_{\min}$ is determined using the mass flow rate and the specific heat capacity c_{p} of the cold and hot stream

$$C_{\min} = \min\left(\dot{m}_c c_{\mathrm{p,c}}, \dot{m}_{\mathrm{h}} c_{\mathrm{p,h}}\right) \tag{2.6}$$

In order to calculate the effectiveness the number of transfer units (NTU) must be determined. It is a measurement of the capacity of transferring heat between the streams, limited by medium with $C_{\min}$

$$\mathrm{NTU} = \frac{UA}{C_{\min}} \tag{2.7}$$

The effectiveness is computed depending on the properties of the heat exchanger. The general expression for a counterflow heat exchanger is formulated as

$$\epsilon = \frac{1 - e^{(-\mathrm{NTU}(1-\mathrm{C_{ratio}}))}}{(1 - \mathrm{C_{ratio}})e^{(-\mathrm{NTU}(1-\mathrm{C_{ratio}}))}} \tag{2.8}$$

where $\mathrm{C_{ratio}}$ is the heat capacity ratio $C_{\min}/C_{\max}$. If one stream is boiling or condensing the heat capacity ratio effectively is infinite. Letting $\mathrm{C_{ratio}}$ approach 0 yields the simplified expression of this heat exchange configuration

$$\epsilon_{\mathrm{phaseShift}} = 1 - \mathrm{e}^{-\mathrm{NTU}} \tag{2.9}$$

This is however not valid in the radiator which is a crossflow heat exchanger. Neither the flow of air nor the coolant is a mixture and the effectiveness can therefore be formulated as

$$\epsilon_{\mathrm{cross}} = (1 + 0.44(1 - C_{\mathrm{ratio}}))(1 - (0.92 + (\pi C_{\mathrm{ratio}}^{0.15}\mathrm{NTU})^{1.25})^{-0.4}) \tag{2.10}$$

when $\mathrm{C_{ratio}} > 0.3$ and $\mathrm{NTU} > 1$. Otherwise, the effectiveness is defined as

$$\epsilon_{\mathrm{cross}} = 1 - e^{(e^{-C_{\mathrm{ratio}}^{1.15}\mathrm{NTU}} - 1)/C_{\mathrm{ratio}}^{1.15}} \tag{2.11}$$

2.4 Model adjustments

With the test vehicle being a prototype as described in Section 2.1.1, the performance of its system deviates from the expected result. This affects the simulation model since the predicted outcome is not equal to the observed one.

2.4.1 Velocity dependency

The test vehicle is not fully developed and the flaws will be modified at a later stage, but requires to be accounted for in the model to represent the current vehicle status.

For instance, the components in the TEM system utilizing ambient air to transfer heat suffer from inconsistent data. That is the radiator in the coolant circuit and the evaporator and ACC in the refrigerant circuit, as seen in Figure 2.1. The intake of ambient air increases with the velocity as more air passes the vehicle. The software estimations of the air mass flow have trouble compensating for this, causing a less reliable estimate. The software uses the speed of the fan placed in front of the component to estimate the air mass flow rate. Moreover, the defect also influences the inlet temperature used to compute the heat transfer from the incorrect mass flows.

Since the radiator uses ambient air to extract heat, the increased mass flow rate will not affect the inlet temperature of the air blown over the radiator. The estimated mass flow deviates more from reality as the speed of the car increases. Figure 2.3 illustrates the speed profile used to collect the measurements. Therefore the model is adjusted such that the air mass flow over the radiator is dependent on the velocity.

Similar to the radiator, the ACC uses ambient air to exchange heat. The leakage increases the mass flow of air over the ACC as the velocity increases. The evaporator on the other hand uses the recirculation door to regulate the ratio of air, which is illustrated in Figure 2.1. Depending on the position of the door, the increased air flow affects both the mass flow of air and its inlet temperature. If the door is fully open all air blown over the evaporator is recirculated from the cabin. If the door instead is closed, all air is taken from the ambient, and only the mass flow rate is affected. For scenarios between these endpoints, both the mass flow and temperature will be affected.

2.4.2 Heat transfer with phase change

In heat exchangers where one of the fluids is changing phase, the effectiveness-NTU method described in Section 2.3 has to be modified. With the thermal capacity of the phase shifting fluid then becoming infinitely large, it results in the effectiveness as Equation 2.9 [12]. With the refrigerant having phase shift it is not the limiting medium nor influences the effectiveness value. As described in Section 2.4.1 the estimations of air mass flows are unreliable and underestimated. Basing the heat exchange on these estimations, being the limiting medium, would result in incorrect temperatures for both refrigerant but also air entering the cabin. An alternative method is then required to estimate the heat transfer between the two mediums.

As the refrigerant first shifts phase followed by a temperature change, the heat transfer can be separated into two segments. With knowledge of the characteristics of the refrigerant, the energy required for the mass flow to complete a phase shift can be calculated. The second segment can utilize the effectiveness-NTU method as the specific heat capacity at this point is limited. With the unreliable value for the air mass flow, the limiting medium is set to be the refrigerant. The two segments combined represent the total energy transferred in the heat exchange.

3
System Modeling

This chapter utilizes the theory from Section 2 to represent the system in a mathematical model. The system is divided into two subsystems, that is the coolant and refrigerant circuit, with the explanation of the heat exchange between these and the vehicle surroundings. Respective circuits are validated separately to determine their performance. Further, the simplifications introduced in the model are presented.

The TEM system is visualized in Figure 3.1 with the inputs and outputs of the plant model marked in the figure.

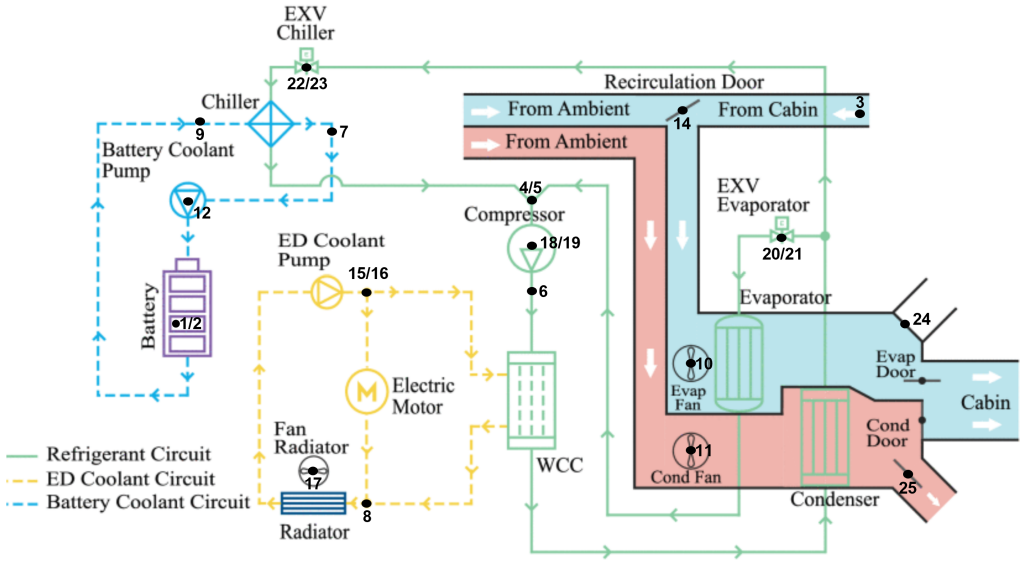

Figure 3.1: Overview of the CTEM system with input and output signals

Table 3.1 and 3.2 present the inputs and outputs of the plant model together with the abbreviation used in the system modeling.

Table 3.1: Outputs of the plant model

Number	Variable name	Abbreviation	Unit
1	State of charge	Soc	%
2	Battery temperature	T_{batt}	$°C$
3	Cabin air temperature	T_{cabin}	$°C$
4	Compressor suction pressure	P_s	Bar
5	Suction refrigerant temperature	T_s	$°C$
6	Compressor discharge pressure	P_d	Bar
7	Chiller coolant temperature out	$T_{\text{chillClntOut}}$	$°C$
8	Radiator coolant temperature out	$T_{\text{radClntOut}}$	$°C$
9	Chiller coolant temperature in	$T_{\text{chillClntIn}}$	$°C$

Table 3.2: Inputs to the plant model

Number	Variable name	Abbreviation	Unit
10	Evaporator mass flow	$\dot{m}_{\text{evapAir}}$	kg/s
11	ACC mass flow	$\dot{m}_{\text{accAir}}$	kg/s
12	Battery pump speed	-	%
-	Cooling mode	-	1
14	Air re-circulation	b_{rec}	%
15	Electric drive coolant mass flow	$\dot{m}_{\text{edClnt}}$	kg/s
16	Water cooled condenser mass flow	$\dot{m}_{\text{wccClnt}}$	kg/s
17	Radiator mass flow	$\dot{m}_{\text{radAir}}$	kg/s
18	Compressor speed	ω	rev/min
19	Compressor acceleration	$\dot{\omega}$	rev/min^2
20	EXV evaporator position	z_{evap}	%
21	Rate of EXV evaporator position	$\dot{z}_{\text{evap}}$	%/s
22	EXV chiller position	z_{chill}	%
23	Rate of EXV chiller position	$\dot{z}_{\text{chill}}$	%/s
24	Waste cold air	b_{cold}	Boolean
25	Waste hot air	b_{hot}	Boolean

The order in which the plant model computes its properties is illustrated by a flow chart in Figure 3.2 below. With the blue section representing the coolant subsystem and the green section the refrigerant circuit.

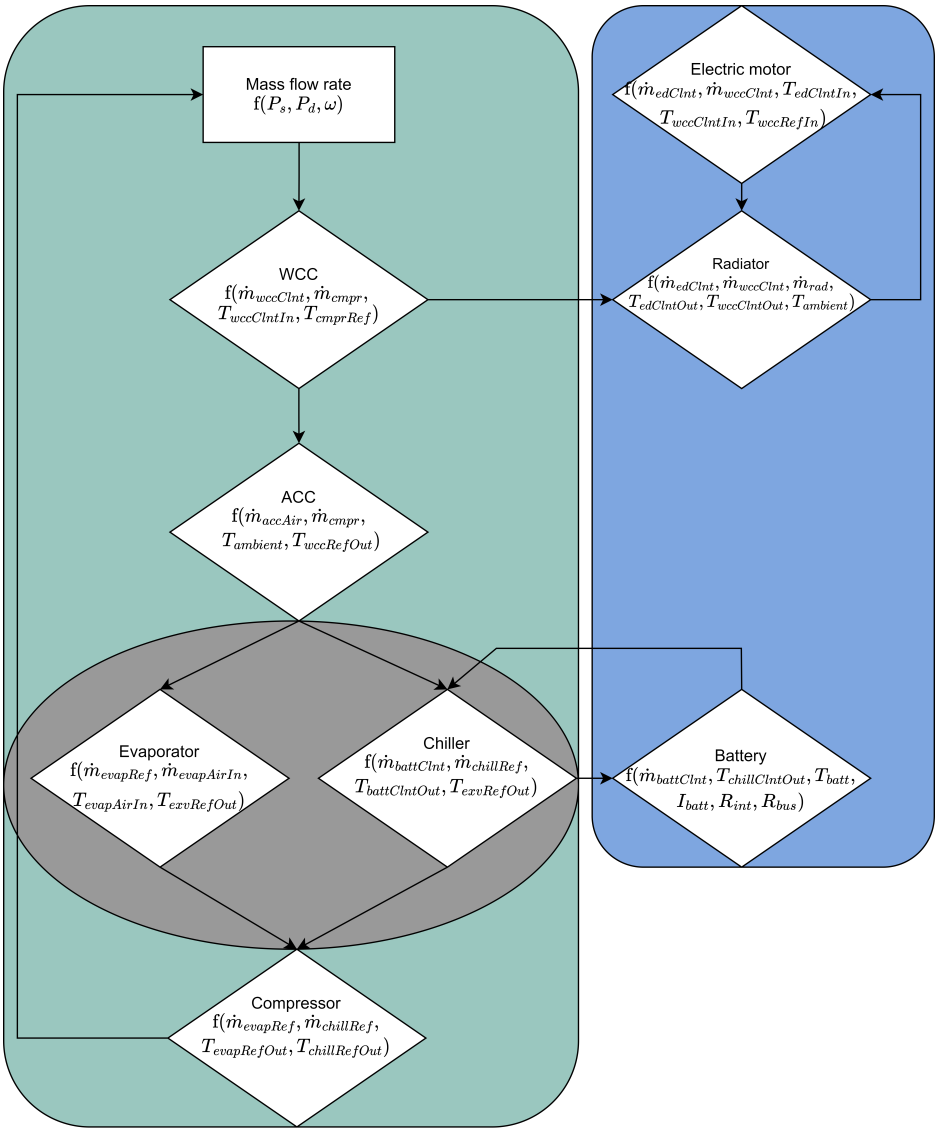

Figure 3.2: Flow chart of the TEM system with refrigerant circuit depicted in green and coolant in blue.

3.1 Simplifications

The model of the system is designed to mirror the physical system with some areas having alternative approaches which simplify and restrict the problem. Firstly the system is assumed to have the correct level of refrigerant meaning that the system will not divert from its expected behavior by having refrigerant accumulate or having a smaller amount and not meet the cooling needs. It is therefore possible to assume the quality of the refrigerant at the evaporator's inlets to be constant. The quality line used in Section 3.3.1 is a constant in the model. The refrigerant circuit is also divided by its pressure into two subsystems with a low and high side separated by the compressor and the expansion valves. Each subsystem is assumed to have a constant pressure over one iteration. Meaning that the pressure is equal over all components, on the high side and low side respectively. It is also assumed that there are no temperature losses in the tubes in between components.

Out of the three stages of condensation described in Section 2.2.1.3, the model assumes the de-superheating to take place in the WCC. With the phase transition and sub-cooling taking place in the ACC. The suction pressure could be calculated by the enthalpy change if the refrigerant in between the time steps. Due to unreliable values to compute heat transfer rate throughout the model and sensitive it being sensitive ti larger deviations. The model updates it pressure based on the EXV positions and the compressor speed seen in Section 3.3.2.2, this simplification restricts the model from picking up all the system dynamics.

The system has two expansion valves controlling the refrigerant flow over the chiller and evaporator with their opening areas adjusting the pressure difference over the EXVs which is described in Section 2.2.2. How the pressure drop is calculated over two parallel valves individually is not represented in the literature, however, it is described for one valve. As the pressure difference is calculated from the opening area separating the high and low sides, the valves are modeled as one opening area with the two valves combined as one. The refrigerant temperature after expanding at the low side of the EXVs is related to pressure and the specific enthalpy. With losses disregarded in between components, the enthalpy out from the EXVs is equal to the one exiting the ACC. To prevent the system to drift from its vapor-compression cycle the lower left corner in Figure 2.5 is fixed to a quality line, assuming that the ratio of gas to liquid remains constant.

3.2 Coolant circuit

As described in section 2.1 the coolant circuit can be altered between four different modes which enables the system to operate more efficiently in all climates. The components are not modified by the mode change. Instead, it only affects the flow of the coolant to change where the excess heat is diverted to.

The coolant side is designed with three states of temperatures, being inlet and outlet from the chiller and outlet to the radiator. The reason for using two states on the chiller is traced back to the refrigerant side where there is no measurement of the

true temperature on the inlet. By isolating the chiller and knowing three states it is possible to verify that the model outputs are correct and also the estimated inlet refrigerant temperature which is described in section 3.3.

3.2.1 Electric drive circuit

The losses in the electric motor are mapped from inputs of vehicle speed and road gradient and are considered to generate heat in the motor itself. This results in an estimated temperature of the motor which will exchange heat with the flowing coolant. The effectiveness in the transfer between the solid metal and the liquid is dependent on the $\dot{m}_{\text{edClnt}}$, an increased flow will be less effective for the same contact area but still achieve a larger heat exchange. Since there is no phase shift in the coolant it can be considered that all the transferred energy results in a change in temperature for both mediums. The exchange is limited by the coolant and the transferred energy can be calculated as

$$\dot{Q}_{\text{em}} = \epsilon_{\text{em}}\, c_{\text{p,em}} \dot{m}_{\text{edClnt}} (T_{\text{em}} - T_{\text{emClntIn}}) \tag{3.1}$$

where $c_{\text{p,em}}$ is the specific heat capacity for the coolant liquid and ϵ_{em} is the effectiveness in the exchange. The coolant temperature out from the electric motor is given as the temperature change added to the inlet temperature as

$$T_{\text{emClntOut}} = T_{\text{emClntIn}} + \frac{\dot{Q}_{\text{em}}}{c_{\text{p,clnt}} \dot{m}_{\text{edClnt}}} \tag{3.2}$$

The second heat exchange in the coolant circuit is in the WCC where the coolant liquid interacts with the refrigerant gas which is superheated such that it will not experience phase shift. Since the only known states are the two inlet temperatures the effectiveness-NTU method described in Section 2.3 is used to model the exchange, the flow rate of the two mediums is decisive to the limiting factor which impacts the effectiveness. The energy transferred is calculated as

$$\dot{Q}_{\text{wcc}} = \epsilon_{\text{wccCross}}\, C_{\text{min}} (T_{\text{d}} - T_{\text{radClntOut}}) \tag{3.3}$$

$$T_{\text{wccClntOut}} = T_{\text{radClntOut}} + \frac{\dot{Q}_{\text{wcc}}}{c_{\text{p,clnt}} \dot{m}_{\text{wccClnt}}} \tag{3.4}$$

The ambient air is used to remove unwanted heat from the cooling liquid over the radiator which is wasted from the system. In the same way as before the effectiveness-NTU method is used to estimate the heat exchanged between the two mediums, which is changed with no phase transition meaning that the effectiveness is calculated as Equation 2.10 - 2.11. The fan speed can be adjusted to update the flow rate of air, a factor to keep in mind is the temperature of the air which restricts the lowest temperature the coolant can reach. T_{airOut} is not of interest since it is wasted to the ambient air, but the rate of heat exchange in the radiator is computed as

$$\dot{Q}_{\text{rad}} = \epsilon_{\text{radCross}}\, C_{\text{min}} (T_{\text{ambientAir}} - T_{\text{radClntIn}}) \tag{3.5}$$

Determine the inlet temperature to the radiator is dependent on the cooling mode. In warmer ambient conditions, as illustrated in Figure 2.1, the inlet temperature is calculated from the coolant at the WCC outlet and electric motor outlet

$$T_{\text{radClntIn}} = \frac{\dot{m}_{\text{edClnt}} T_{\text{emClntOut}} + \dot{m}_{\text{wccClnt}} T_{\text{wccClntOut}}}{\dot{m}_{\text{edClnt}} + \dot{m}_{\text{wccClnt}}} \tag{3.6}$$

The coolant outlet temperature $T_{\text{radClntOut}}$ is then

$$\begin{aligned} T_{\text{radClntOut}} =& T_{\text{radClntIn}} + \frac{\dot{Q}_{\text{rad}}}{c_{\text{p,clnt}}(\dot{m}_{\text{wccClnt}} + \dot{m}_{\text{edClnt}})} \\ &+ x_1 \text{v}^2 (T_{\text{ambientAir}} - T_{\text{radClntIn}}) \end{aligned} \tag{3.7}$$

where the last term account for the leakage caused by the velocity, which is described in Section 2.4.1, and x_1 is the velocity correction factor.

3.2.1.1 Validation of electric drive subsystem

This section presents the result of the ED circuit for an ambient temperature of -10°C, 0°C, 40°C, and 45°C. The components of interest are the coolant temperature at the inlet and outlet of the radiator and the coolant temperature at the WCC outlet.

Ambient temperature -10°C

The inlet of the radiator has a constant offset illustrated in Figure 3.3 with measurement of the radiator inlet showing unreliable values as measurements both before and after is indicating a lower temperature. Since only the battery increases the coolant temperature in between also has a lower temperature than indicated by the radiator inlet. The modeled radiator overestimates the effect of vehicle velocity at the final third of the cycle where the velocity increases.

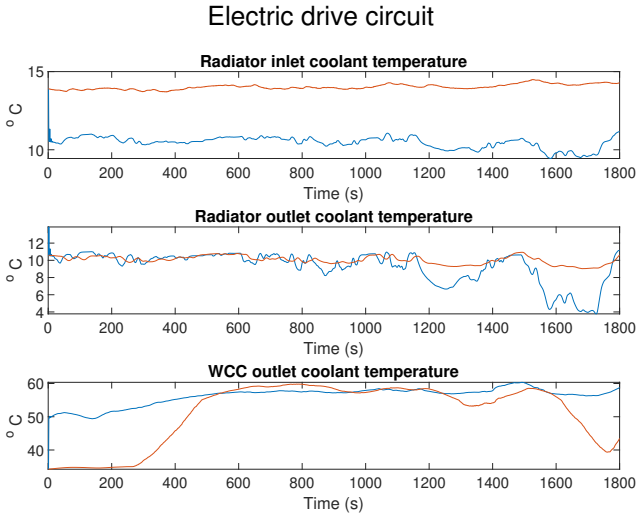

Figure 3.3: Output from the electric drive circuit of the isolated coolant subsystem with ambient temperature -10°C. The red line corresponds to the measurement and the blue line is the model estimation.

Ambient temperature 0°C

There is a periodic pattern in the electric drive circuit caused by the refrigerant side where the chiller EXV is opening and closing to control the pressure and mass flow. In Figure 3.4 it can be seen that WCC is underestimating the temperature at the same as the chiller inlet is overestimated which indicates that the divided flow over the electric motor and WCC is incorrect. The periodic peaks in the chiller inlet correlate with increasing velocity and load on the electric motor, suggesting the developed heat in the electric motor transferred to the coolant is overestimated.

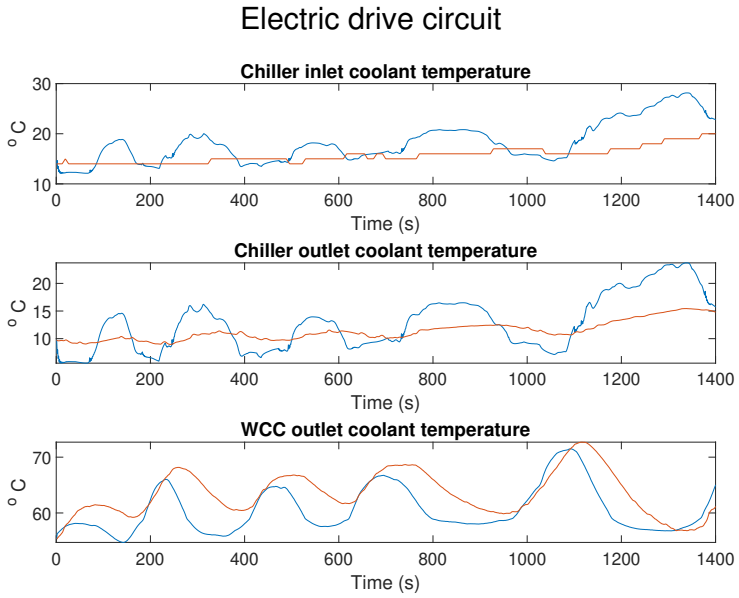

Figure 3.4: Output from the electric drive circuit of the isolated coolant subsystem with ambient temperature 0°C. The red line corresponds to the measurement and the blue line is the model estimation.

Ambient temperature 40°C

The temperature at the radiator in- and outlet is higher than the measurement while the WCC outlet is lower. This indicates that the flow over the electric motor is generating too much heat which increases the overall temperature in the circuit seen in figure 3.5. On the other hand, the WCC outlet is lower than its reference which suggests that the estimated flow is too large such that the distribution of the two flows is incorrect. A smaller flow over the electric motor also results in the system not removing enough heat from the electric motor.

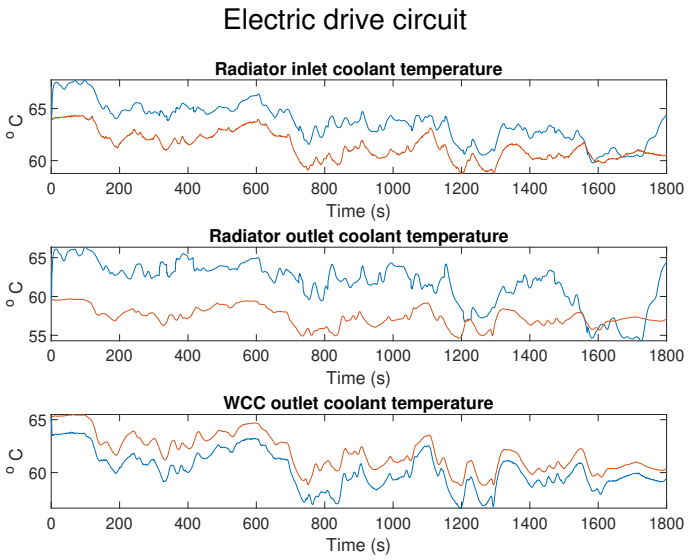

Figure 3.5: Output from the electric drive circuit of the isolated coolant subsystem with ambient temperature 40°C. The red line corresponds to the measurement and the blue line is the model estimation.

Ambient temperature 45°C

With similar conditions to the use case of 40°C in Section 3.2.1.1 the results model behavior is as expected close to the measurement seen in Figure 3.6.

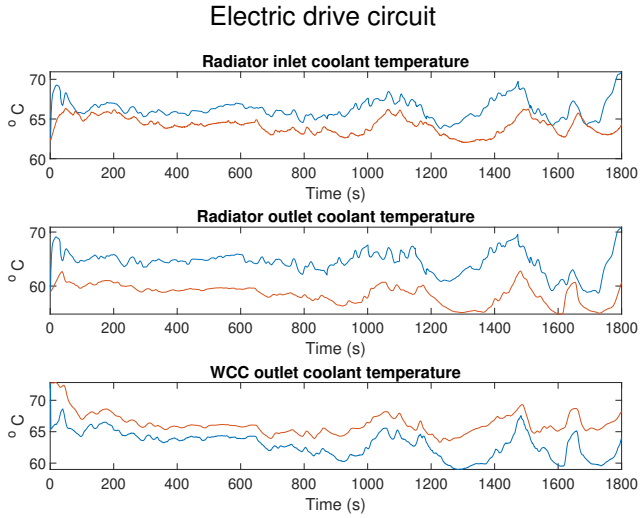

Figure 3.6: Output from the electric drive circuit of the isolated coolant subsystem with ambient temperature 45°C. The red line corresponds to the measurement and the blue line is the model estimation.

The root mean squared (RMS) errors of the electric drive circuit are listed in Table 3.3 below. The temperatures were the mass flow of coolant is stagnant is omitted. Based on the cooling demand some signals are excluded as they are not present.

Table 3.3: RMS error for the electric drive circuit of the isolated coolant subsystem

RMSE / Signal	-10	0	40	45
$\mathbf{T_{chillClntIn}}$	-	3.9899	-	-
$\mathbf{T_{chillClntOut}}$	-	3.8401	-	-
$\mathbf{T_{radClntIn}}$	3.5862	-	2.4151	2.4566
$\mathbf{T_{radClntOut}}$	1.6644	-	5.0066	6.2127
$\mathbf{T_{wccClntOut}}$	8.5829	4.2335	1.6921	3.5345

3.2.2 Battery circuit

A battery is developing heat for multiple reasons when it is discharged or charged, partly from chemical reactions inside the battery but also from power losses over its resistance which is in relation to the current and resistance [13], [14]. The losses are simplified to only include the power losses and are calculated below with R_{int} being the internal battery resistance, R_{bus} the bus bar resistance which is the connections between the battery cells and I_{batt} the battery current. The heat developed in the battery is calculated as

$$\dot{Q}_{\text{generative}} = I_{\text{batt}}^2(R_{\text{int}} + R_{\text{bus}}) \tag{3.8}$$

The cooling of the battery is controlled by the coolant flow quantity with the heat transfer being calculated in the same way as the electric motor in Section 3.2.1. The heat exchange is dependent on temperature difference and is calculated as

$$\dot{Q}_{\text{cool}} = \epsilon_{\text{batt}}\, \dot{m}_{\text{battClnt}} c_{\text{p,clnt}}(T_{\text{batt}} - T_{\text{battClntIn}}) \tag{3.9}$$

The temperature of the battery and coolant liquid after the exchange is updated as

$$T_{\text{battClntOut}} = T_{\text{battClntIn}} + \frac{\dot{Q}_{\text{cool}}}{\dot{m}_{\text{battClnt}} c_{\text{p,clnt}}} \tag{3.10}$$

$$T_{\text{batt}} = T_{\text{batt}} + \frac{\dot{Q}_{\text{generative}} - \dot{Q}_{\text{cool}}}{\text{m}_{\text{batt}} c_{\text{p,batt}}} \tag{3.11}$$

The coolant liquid increases in temperature when flowing through the battery and will offload its heat at the chiller before returning to the battery once again. The heat exchange between the coolant and refrigerant side includes a phase transition on the refrigerant side while the coolant only changes temperature which is described in Section 3.3.1.2.

The level of charge in the battery is decreasing as energy is taken out from it. The rate of change is dependent on the current and the battery's nominal capacity. When breaking, electric vehicles regenerate power from the motor which increases the battery charge. The SoC is updated as

$$\text{SoC}_{\text{new}} = \text{SoC} - \frac{I_{\text{batt}}}{Q_{\text{nom}}} \tag{3.12}$$

where I_{batt} and Q_{nom} is the battery current and its nominal capacity.

3.2.2.1 Validation of battery circuit subsystem

This section presents the result of the battery circuit for an ambient temperature of -10°C, 0°C, 40°C, and 45°C. The components of interest are the coolant temperature at the inlet and outlet of the chiller and the temperature of the battery.

Ambient temperature -10°C

The battery and the in- and outlet temperatures of the chiller are initially close to its references seen in Figure 3.7. The deviation increases towards the end of the cycle with a correlation to the vehicle velocity increasing during the same period of time.

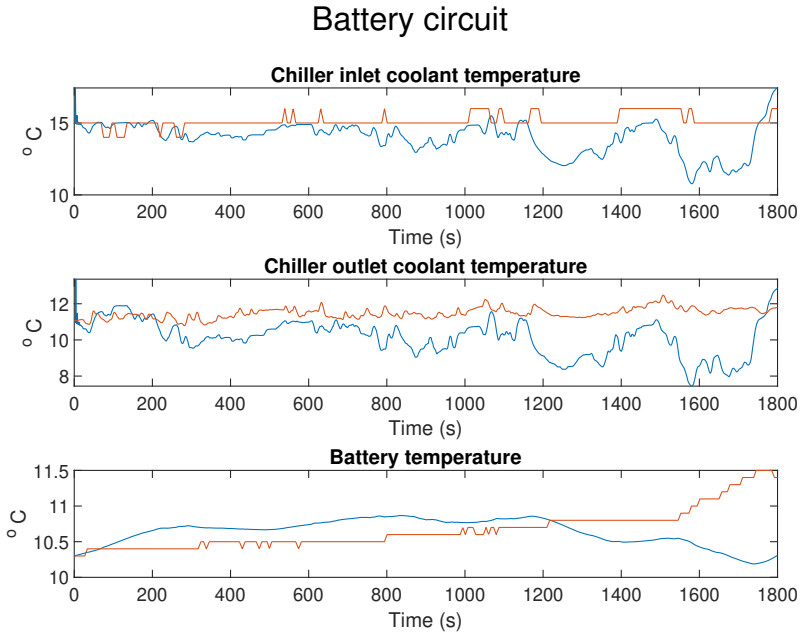

Figure 3.7: Output from the battery circuit of the isolated coolant subsystem with ambient temperature -10°C. The red line corresponds to the measurement and the blue line is the model estimation.

Ambient temperature 0°C

In cold ambient temperatures, the battery is not in the same need for cooling. Depending on the battery's temperature, the cold ambient air can be sufficient to keep it in its operating window. In fact, the pump controlling the cooling flow is switched off causing a standing liquid and the battery temperature is close to its reference seen in Figure 3.8.

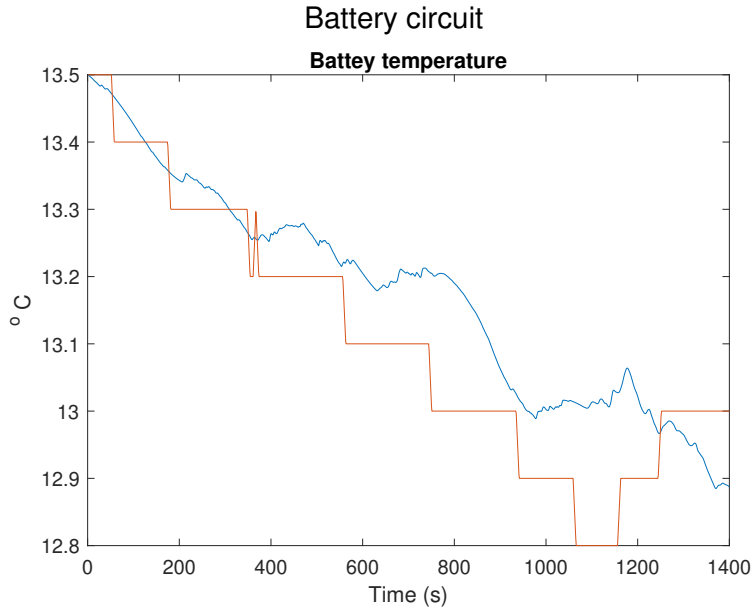

Figure 3.8: Output from the battery circuit of the isolated coolant subsystem with ambient temperature 0°C. The red line corresponds to the measurement and the blue line is the model estimation.

Ambient temperature 40°C

With a high ambient temperature, the battery requires resources for cooling to maintain a stable operating point. The overall temperature in the circuit increases including the battery shown in Figure 3.9 with the model following its reference.

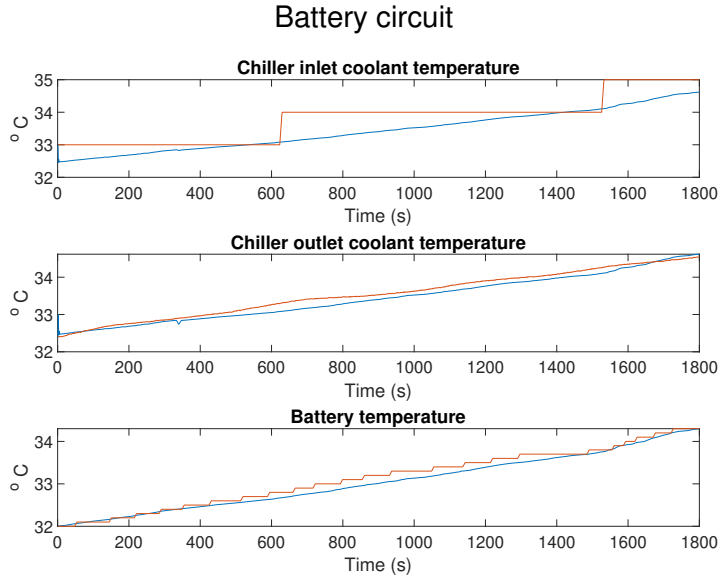

Figure 3.9: Output from the battery circuit of the isolated coolant subsystem with ambient temperature 40°C. The red line corresponds to the measurement and the blue line is the model estimation.

Ambient temperature 45°C

The small difference in conditions from 40°C in Section 3.2.2.1 has the system operating in a similar way and the model is able to follow its reference as seen in Figure 3.10.

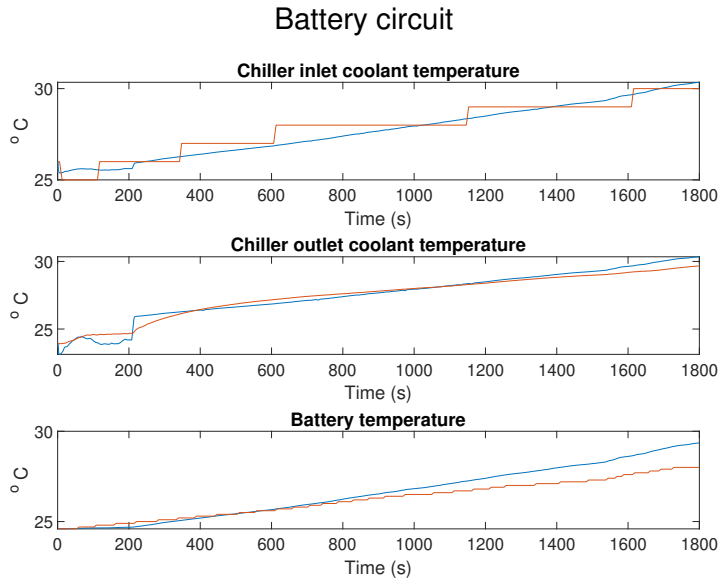

Figure 3.10: Output from the battery circuit of the isolated coolant subsystem with ambient temperature 45°C. The red line corresponds to the measurement and the blue line is the model estimation.

Table 3.4 shows the RMS error of the battery circuit for the isolated coolant subsystem. At 0°C the coolant flow is stagnant and the temperature of the coolant at the chiller inlet and outlet is omitted.

Table 3.4: RMS error for the battery circuit of the isolated coolant subsystem

RMSE / Signal	-10	0	40	45
$\mathbf{T_{chillClntIn}}$	1.6052	-	0.4541	0.4423
$\mathbf{T_{chillClntOut}}$	1.7087	-	0.1284	0.3554
$\mathbf{T_{batt}}$	0.4134	0.1037	0.1160	0.5834

3.3 Refrigerant circuit

The processes in the vapor-compressor cycle are described in Section 2.2. In contrast to the coolant circuit, the modeling of the refrigerant circuit is independent of the coolant modes, except that the origin of the coolant into the WCC and chiller differs. The model of the refrigerant system makes use of three states, namely the compressor suction pressure P_s, suction refrigerant temperature T_s, and thirdly the compressor discharge pressure P_d.

3.3.1 Evaporation

The evaporators provide the system with the required cooling effect. Where the evaporator cools the air entering the cabin whereas the chiller absorbs excessive heat from the coolant in the chiller. In order to estimate T_s it is needed to determine the outlet temperature of the chiller and evaporator. Which in turn depend on several variables, as illustrated in Figure 3.11 below.

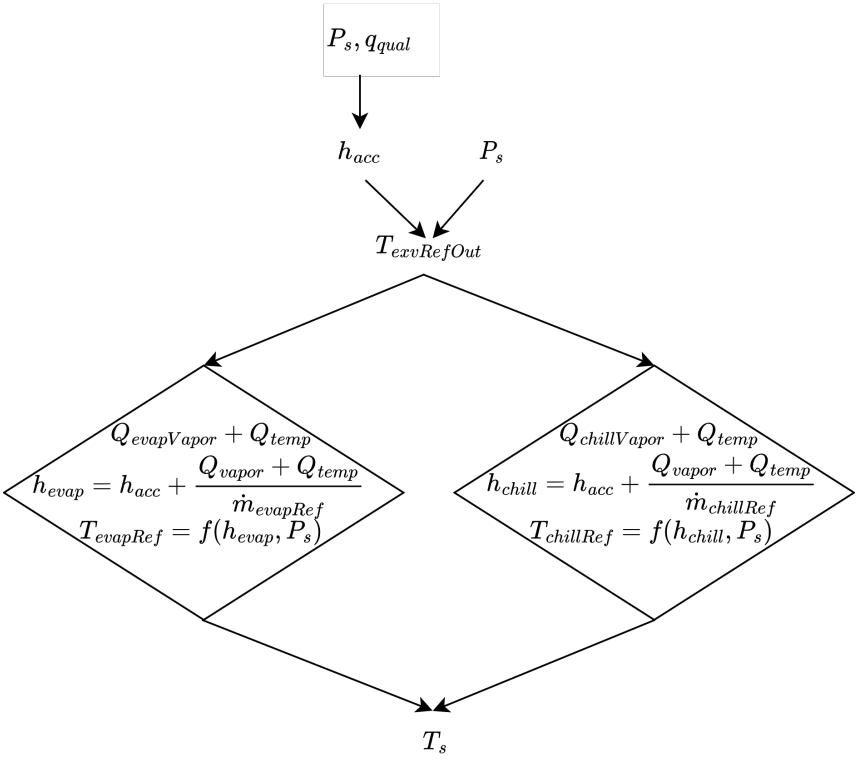

Figure 3.11: Detailed flow chart of the evaporation being the grey area in Figure 3.2

The mass flow of refrigerant pumped from the compressor is divided over the chiller and evaporator after exiting the ACC which can be seen in Figure 3.1. How the flow is distributed depends on the EXV positions and is computed as

$$\dot{m}_\mathrm{evapRef} = \frac{z_\mathrm{evap}}{z_\mathrm{evap} + z_\mathrm{chill}} \dot{m}_\mathrm{cmpr} \quad \text{and} \quad \dot{m}_\mathrm{chillRef} = \frac{z_\mathrm{chill}}{z_\mathrm{evap} + z_\mathrm{chill}} \dot{m}_\mathrm{cmpr} \tag{3.13}$$

The temperature of the refrigerant leaving the EXV and entering the chiller and evaporator is interpolated according to Figure 3.2. $T_\mathrm{exvRefOut}$ is determined using the specific enthalpy at the ACC outlet and the suction pressure

$$T_\mathrm{exvRefOut} = f(h_\mathrm{acc}, P_\mathrm{s}) \tag{3.14}$$

3.3.1.1 Evaporator

In the initial phase of the heat exchange, the refrigerant in the evaporator will absorb heat from the air without an increase in its temperature. All heat transferred

between the streams leads to a phase change of the refrigerant, when in the two-phased region. The heat transfer rate which vaporizes the refrigerant is computed as

$$\dot{Q}_{\text{evapVapor}} = \Delta h_{\text{evapVapor}} \dot{m}_{\text{evapRef}} (1 - q_{\text{qual}}) \tag{3.15}$$

where $\Delta h_{\text{evapVapor}}$ is the specific enthalpy required to vaporize the refrigerant for a given temperature and q_{qual} is the quality line in the mixed region. The heat exchange which changes the refrigerant's phases is assumed to occur without losses. It means that the effectiveness is 1 and the exchange is not limited by any of the flows. When the refrigerant is saturated vapor the heat exchange will increase the temperature of the refrigerant. This process is computed using the effectiveness-NTU method derived in Section 2.3. The effectiveness in the evaporator is calculated according to Equation 2.9 leading to the heat transfer rate computed as

$$\dot{Q}_{\text{evapTemp}} = \epsilon_{\text{evapPhaseShift}} C_{\min} \left(k_{\text{evap}} T_{\text{evapAirIn}} - T_{\text{exvRefOut}} \right) \tag{3.16}$$

where k_{evap} is a constant accounting for the decrease of $T_{\text{evapAirIn}}$ during the phase shift. The refrigerant mixture have constant temperature during the vaporization, whereas the gaseous air does not undergo phase change. Furthermore, using the energy balance and the total heat transfer, $\dot{Q}_{\text{totEvap}} = \dot{Q}_{\text{evapVapor}} + \dot{Q}_{\text{evapTemp}}$, the outlet temperatures can be solved. The outlet temperature of the air which cools the vehicle cabin is computed

$$T_{\text{evapAirOut}} = T_{\text{evapAirIn}} - \frac{\dot{Q}_{\text{totEvap}}}{\dot{m}_{\text{evapAir}} c_{\text{p,air}}} \tag{3.17}$$

The temperature of the superheated vapor at the evaporator outlet is computed from the enthalpy change according to Figure 3.11

$$h_{\text{evapRefOut}} = h_{\text{acc}} + \frac{\dot{Q}_{\text{totEvap}}}{\dot{m}_{\text{evapRef}}} \tag{3.18}$$

where h_{acc} is the specific enthalpy at the evaporator inlet. The temperature at the outlet is then interpolated from $h_{\text{evapRefOut}}$ and the suction pressure

$$T_{\text{evapRefOut}} = f \left(h_{\text{evapRefOut}}, P_{\text{s}} \right) \tag{3.19}$$

3.3.1.2 Chiller

The heat transfer rate in the chiller is computed similarly to the heat exchange in the evaporator described in Section 3.3.1.1. The majority of the energy is used to vaporize the refrigerant, but it absorbs heat from the coolant circuit instead of air. The heat transfer rate to vaporize the refrigerant is calculated as

$$\dot{Q}_{\text{chillVapor}} = \Delta h_{\text{chillVapor}} \dot{m}_{\text{chillRef}} (1 - q_{\text{qual}}) \tag{3.20}$$

where the mass flow rate of refrigerant over the chiller and evaporator is computed as a percentage of the compressor flow based on respective EXV position. The heat transfer which yields an increased refrigerant temperature

$$\dot{Q}_{\text{chillTemp}} = \epsilon_{\text{chillPhaseShift}} C_{\min} \left(k_{\text{chill}} T_{\text{battClntOut}} - T_{\text{exvRefOut}} \right) \tag{3.21}$$

$T_{\text{battClntOut}}$ is the chiller inlet temperature in one cooling mode, but it varies depending on the mode. The temperature of the coolant at the chiller outlet is computed as

$$T_{\text{chillClntOut}} = T_{\text{battClntOut}} - \frac{\dot{Q}_{\text{totChill}}}{\dot{m}_{\text{chillClnt}} c_{\text{p,clnt}}} \tag{3.22}$$

where $\dot{Q}_{\text{totChill}} = \dot{Q}_{\text{chillTemp}} + \dot{Q}_{\text{chillVapor}}$. The refrigerant undergoes a phase change and therefore the temperature is based on the inlet enthalpy h_{acc} and is at the outlet defined as

$$h_{\text{chillRefOut}} = h_{\text{acc}} + \frac{\dot{Q}_{\text{totChill}}}{\dot{m}_{\text{chillRef}}} \tag{3.23}$$

The outlet temperature is then interpolated based on the suction pressure and computed enthalpy

$$T_{\text{chillRefOut}} = f\left(h_{\text{chillRefOut}}, P_{\text{s}}\right) \tag{3.24}$$

3.3.1.3 Validation of evaporation subsystem

This section presents the result of the evaporator and chiller for an ambient temperature of -10°C, 0°C, 40°C, and 45°C. The components of interest are the refrigerant temperature at the outlet of the evaporator and chiller respectively.

Ambient temperature -10°C

Both the EXV into the chiller and evaporator are open in this driving cycle. The model overestimates the evaporator outlet temperature, whereas it underestimates the refrigerant from the chiller as seen in Figure 3.12.

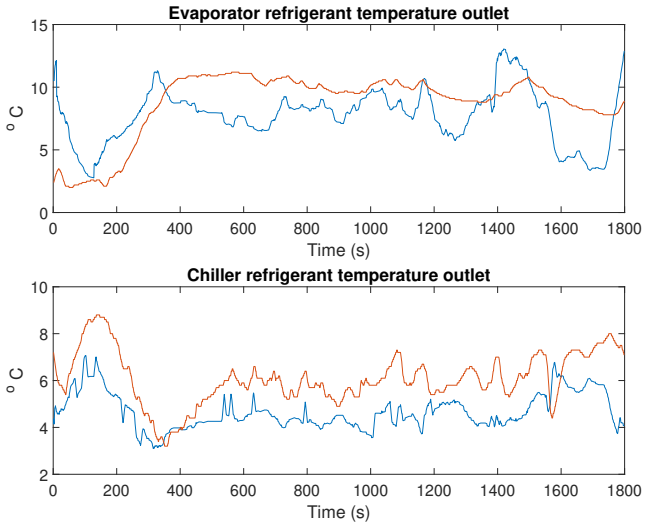

Figure 3.12: Output from the evaporators of the isolated refrigerant subsystem with ambient temperature -10°C. The red line corresponds to the measurement and the blue line is the model estimation.

Ambient temperature 0°C

The EXV opening into the evaporator is constantly 0 throughout the cycle. The valve into the chiller is however open, but it closes around time step 100. At the same time instance, the compressor goes to a halt. As the available data of the compressor do not contain measurements of it standing still the first 400 seconds are removed. Figure 3.13 displays the outlet temperatures of the evaporators, but only the chiller is of interest since the valve into the evaporator is closed. The signals in the driving cycle for 0 °C have a periodic behavior caused by the compressor speed and valve positions. As seen in the figure the model is able to capture this behavior in the chiller outlet temperature.

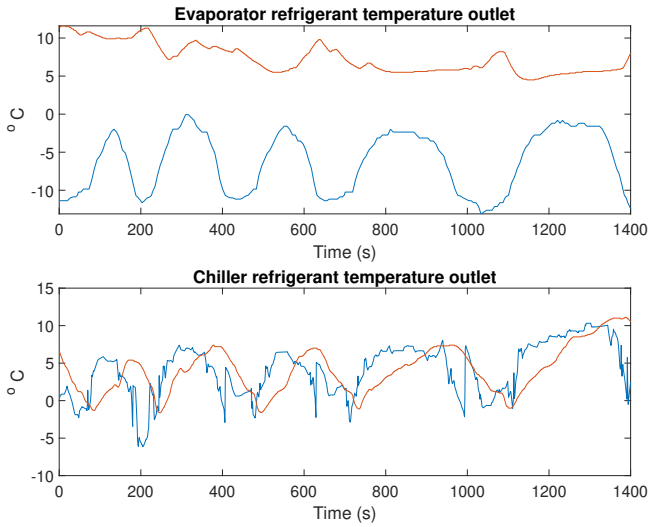

Figure 3.13: Output from the evaporators of the isolated refrigerant subsystem with ambient temperature 0°C. The red line corresponds to the measurement and the blue line is the model estimation.

Ambient temperature 40°C

In the driving cycle with ambient temperature 40°C the EXV into the chiller is instead closed. The battery temperature is not high enough that the circuits need to exchange heat in the chiller. Since the chiller is not utilized its outlet temperature is irrelevant, but it is illustrated for completeness. The EXV into the evaporator on the other is open as the passenger cabin requires cooling. The model is able to capture the trend in the outlet temperate, but not the rapid changes seen in the measured evaporator outlet temperature in Figure 3.14.

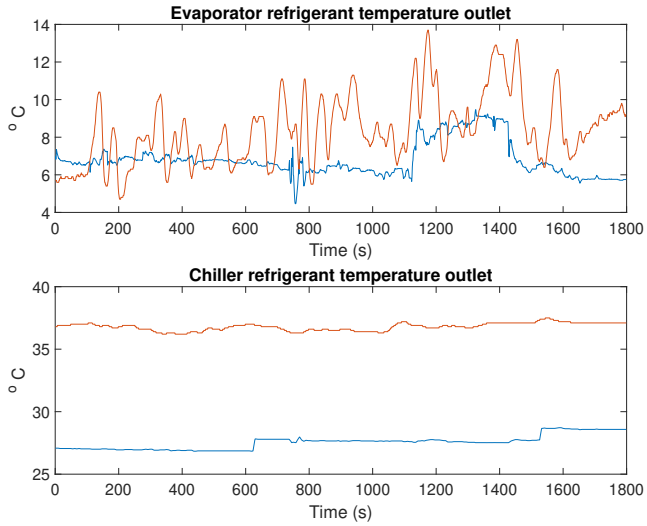

Figure 3.14: Output from the evaporators of the isolated refrigerant subsystem with ambient temperature 40°C. The red line corresponds to the measurement and the blue line is the model estimation.

Ambient temperature 45°C

The cooling needs in this driving cycle are similar to the previous besides that both expansion valves initially are open. The valve into the chiller then closes after approximately 200 seconds and remains closed whereas the evaporator continues to be open, therefore the error in the chiller is left out in Table 3.5. It also utilizes the same constants to determine the pressure difference as the same cooling mode is active. Figure 3.15 shows the evaporator temperature which captures the average refrigerant temperature, but not the fast dynamics. The refrigerant temperature at the chiller outlet initially follows the measurement but deviates with time as the expansion valve limits the mass flow.

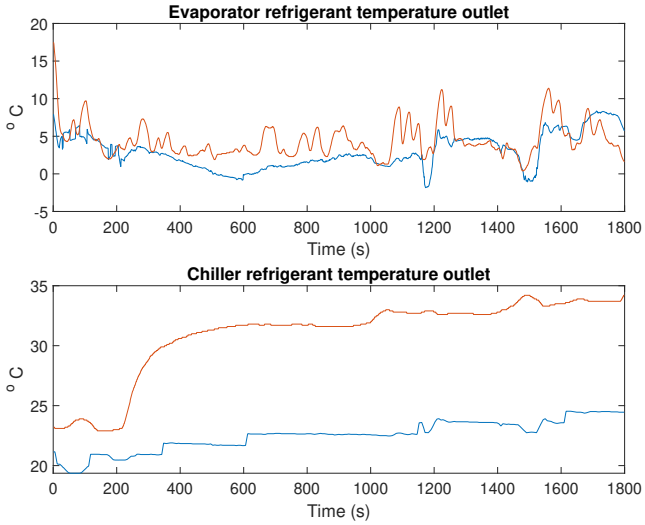

Figure 3.15: Output from the evaporators of the isolated refrigerant subsystem with ambient temperature 45°C. The red line corresponds to the measurement and the blue line is the model estimation.

Table 3.5 show the RMS error for an ambient temperature of 45 °C. The errors which are left out are due to its corresponding expansion valve constantly being closed.

Table 3.5: RMS error for the evaporators of the isolated refrigerant subsystem

RMSE / Signal	-10	0	40	45
$\mathbf{T_{evapRefOut}}$	2.7198	-	2.3858	2.7081
$\mathbf{T_{chillRefOut}}$	1.1076	4.2490	-	-

3.3.2 Pressure calculation

The refrigerant circuit is divided into a high pressure side and low pressure side, as illustrated in Figure 2.5. Where the compressor function to increase the pressure of the refrigerant whereas the EXV expands the medium to maintain the low pressure side. It is assumed that the pressure drop over the refrigerant system components, on the same pressure side, is neglectable. Hence, the pressure drop over the EXV is equivalent to the pressure difference over the compressor.

3.3.2.1 Expansion valve

How the pressure difference over an expansion valve is computed is derived in Section 2.2.2. The first step is to determine the mass flow coefficient C_{D} defined in Equation 3.27. The constants $a_0,\ldots,a_4$ are determined using measurement data and are different for each cooling mode. It is furthermore needed to calculate the subcooling temperature, which in the TEM system is the temperature at the ACC outlet $T_{\mathrm{accRefOut}}$. It is interpolated from data of the refrigerant, and the discharge pressure and specific enthalpy at the ACC outlet. Where the specific enthalpy h_{acc} is interpolated from the suction pressure and quality line

$$h_{\mathrm{acc}} = f\left(P_{\mathrm{s}}, q_{\mathrm{qual}}\right) \tag{3.25}$$

It is not possible to determine $T_{\mathrm{accRefOut}}$ using the change of enthalpy, as done in the evaporator and chiller in Section 3.3.1. The temperature is fully determined by P_{s} and h_{acc} and is interpolated using data of the refrigerant used in the system. Calculating the outlet temperature from the heat exchange would lead to an overdetermined system. Thus the outlet temperature is

$$T_{\mathrm{accRefOut}} = f\left(P_{\mathrm{d}}, h_{\mathrm{acc}}\right) \tag{3.26}$$

It follows that the mass flow coefficient is computed as

$$C_D = a_0 + a_1 z_{\mathrm{tot}} + a_2 z_{\mathrm{tot}}^2 + a_3 z_{\mathrm{tot}} \frac{T_{\mathrm{accRefOut}}}{T_c} + a_4 \frac{T_{\mathrm{accRefOut}}}{T_c} \tag{3.27}$$

where T_{c} is the critical temperature which is a property of the refrigerant, and z_{tot} is the summation $z_{\mathrm{evap}} + z_{\mathrm{chill}}$.

As discussed in Section 2.2.2, the literature predicts the mass flow rate of refrigerant in a system that utilizes one expansion valve [9]. The thermal system in the vehicle however uses two EXV in parallel and Equation 2.3 is therefore adjusted. It is furthermore assumed that the pressure difference over the EXV connected to the chiller is equivalent to the difference over the valve into the evaporator. The valve which yields ΔP is therefore considered one unit with mass flow rate m_{cmpr}

$$\Delta P = \frac{\left(\frac{\dot{\mathrm{m}}_{\mathrm{cmpr}}}{C_d A}\right)^2}{2\rho_s} \tag{3.28}$$

The flow of refrigerant is restricted by the needle and it flows around it as Figure 2.8 illustrates. As the valve is treated as one EXV the flow area A is the sum of the flow area in the chiller and evaporator, denoted d_{chill} and d_{evap}

$$A = D - d_{\mathrm{chill}} + D - d_{\mathrm{evap}} \tag{3.29}$$

3.3.2.2 Compressor

The compressor speed is an input to the plant model and together with the suction and discharge pressure the mass flow rate, m_{cmpr}, is estimated at each time step. It is interpolated using measured data of the compressor for different settings

$$\dot{\mathrm{m}}_{\mathrm{cmpr}} = f\left(P_{\mathrm{d}}/P_{\mathrm{s}}, \omega, P_{\mathrm{s}}\right) \tag{3.30}$$

It is assumed that the pressure drop over the EXV is equivalent to the pressure difference over the compressor. Therefore the suction and discharge pressure can be formulated in terms of ΔP

$$\mathrm{P_d} - \mathrm{P_s} = \Delta P \tag{3.31}$$

In order to calculate the pressure states P_d and P_s an update step is computed in each iteration. The suction pressure is updated from the change in revolutions per minute (RPM), denoted $\dot{\omega}$, and the rate of the EXV position $\dot{z}$ for the two vales

$$P_{\mathrm{s,new}} = k_\mathrm{z}\dot{z} + k_\omega\dot{\omega} \tag{3.32}$$

where k_z and k_ω are constants depending on which cooling mode is used. The valve position controls the rate of refrigerant into the evaporator and chiller and thereby the suction pressure at the low pressure side of the system. Besides increasing the pressure of the vapor from the evaporator and chiller the compressor function to maintain the pressure at the low side [5]. Its capacity is regulated by changing the compressor speed and therefore it affects the suction pressure.

The discharge pressure is determined from the pressure difference ΔP and the updated suction pressure as follows

$$P_{\mathrm{d,new}} = \Delta\mathrm{P} + P_{\mathrm{s,new}} \tag{3.33}$$

The temperature at the compressor inlet is also an output of the plant model. It is estimated from the temperature modeled at the evaporator and chiller outlet, as shown in Figure 3.11. The refrigerant suction temperature is calculated as a percentage of the mass flow through respectively EXV

$$T_\mathrm{s} = \frac{T_{\mathrm{chillRefOut}}\dot{m}_{\mathrm{chillRef}} + T_{\mathrm{evapRefOut}}\dot{m}_{\mathrm{evapRef}}}{\dot{m}_{\mathrm{chillRef}} + \dot{m}_{\mathrm{evapRef}}} \tag{3.34}$$

3.3.2.3 Validation of compressor subsystem

This section presents the result of the pressure calculations for an ambient temperature of -10°C, 0°C, 40°C, and 45°C. The quantities of interest in the compressor are the suction pressure and temperature, and the discharge pressure.

Ambient temperature -10°C

The model of the compressor inlet temperature captures the behavior in the measurement as shown in Figure 3.16. Despite that, the refrigerant temperature at the chiller and evaporator outlet is underestimated and overestimated respectively. The suction pressure is a bit overestimated resulting in a too high suction pressure.

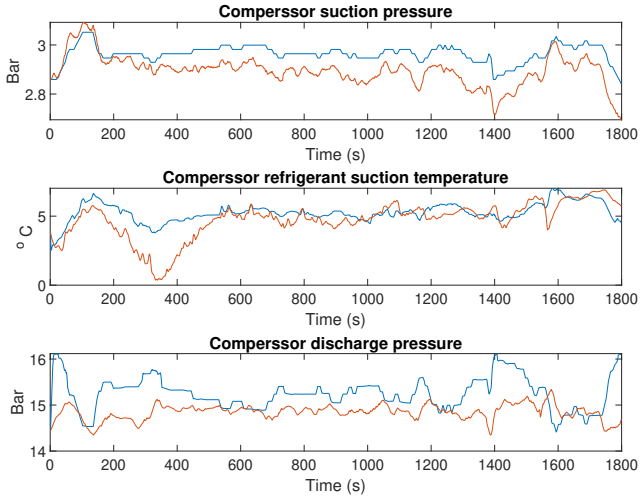

Figure 3.16: Output from the compressor of the isolated refrigerant subsystem with ambient temperature -10°C. The red line corresponds to the measurement and the blue line is the model estimation.

Ambient temperature 0°C

As the chiller temperature is well estimated, and the evaporator is closed, the suction temperature also represents the physical system well. The suction pressure has a small deviation, but the discharge pressure on the other hand has a larger error, as seen in Figure 3.17. The deviation in the estimation of P_s is caused by ΔP being incorrect.

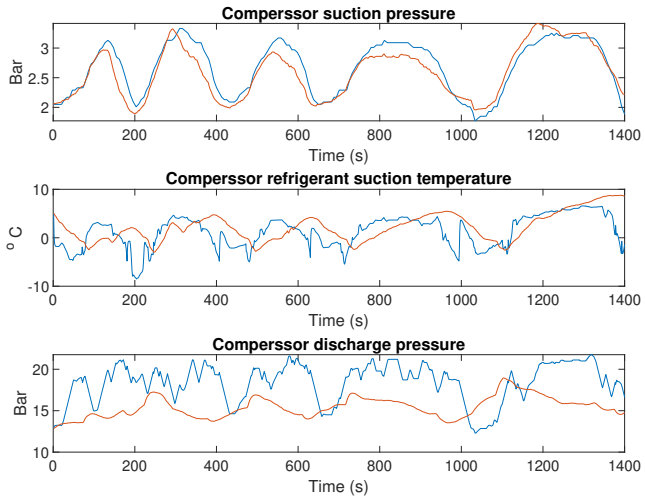

Figure 3.17: Output from the compressor of the isolated refrigerant subsystem with ambient temperature 0°C'. The red line corresponds to the measurement and the blue line is the model estimation.

Ambient temperature 40°C

Both the suction and discharge pressure are underestimated at 40°C which is seen in Figure 3.18. The discharge pressure has an incorrect drop at around 800 seconds caused by a rapid decrease in compressor speed which in turn decreases the estimated mass flow rate $\dot{m}_{cmpr}$. The discharge pressure is updated using ΔP which is sensitive to small deviations in the estimated $\dot{m}_{cmpr}$. It result in an incorrect pressure drop seen in the model output, and not in the the measurement.

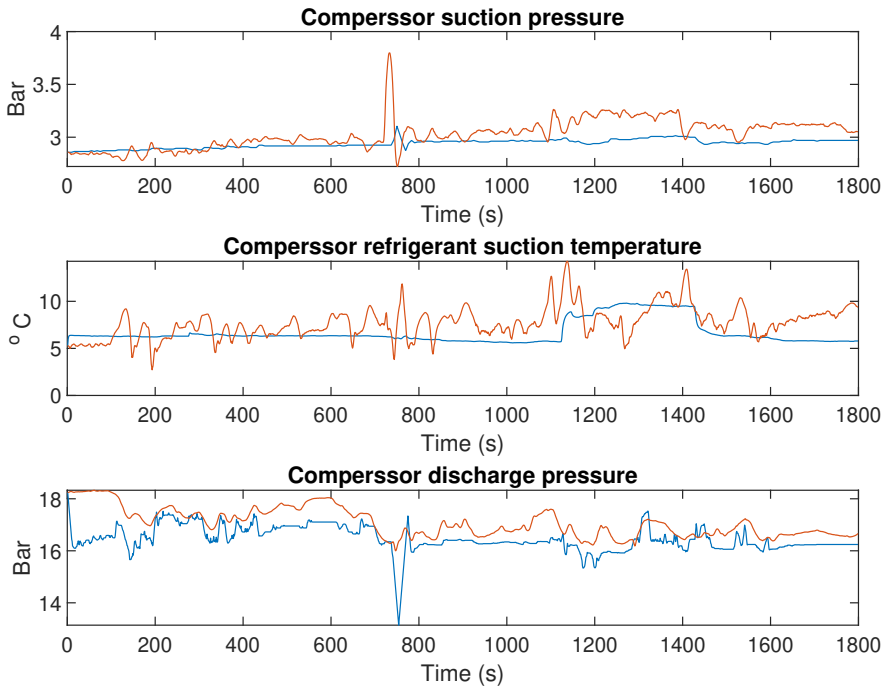

Figure 3.18: Output from the compressor of the isolated refrigerant subsystem with ambient temperature 40°C. The red line corresponds to the measurement and the blue line is the model estimation.

Ambient temperature 45°C

The suction pressure is throughout the cycle overestimated. It is updated using the change in compressor speed and EXV position. As Figure 3.19 shows the pressure does not depend on these properties, the same for both 40°C and 45°C. The suction temperature however follows the trend as well as the discharge pressure. Besides the initial 200 seconds when both expansion valves are open and then the EXV into the chiller closes.

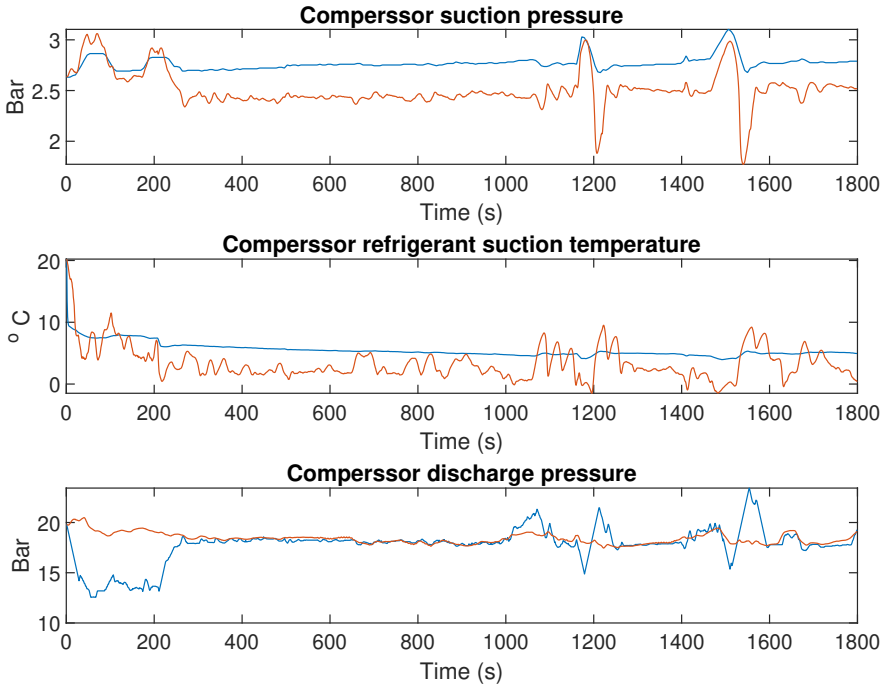

Figure 3.19: Output from the compressor of the isolated refrigerant subsystem with ambient temperature 45°C. The red line corresponds to the measurement and the blue line is the model estimation.

Table 3.6 below shows the RMS error of the compressor pressure and its inlet temperature

Table 3.6: RMS error for the compressor of the isolated refrigerant subsystem

RMSE / Signal	-10	0	40	45
$\mathbf{P_s}$	0.0794	0.1706	0.1477	0.2959
$\mathbf{T_s}$	2.5407	3.4071	1.9659	3.0843
$\mathbf{P_d}$	0.5524	3.4541	0.7783	2.1097

3.3.3 Condensation

The refrigerant system consists of two different types of condensers, namely one water cooled and one air cooled. Besides the different mediums utilized, the difference in modeling the WCC and ACC is to consider the refrigerant change phase. The refrigerant maintains a superheated vapor in the WCC, whereas it condenses to a subcooled liquid in the ACC.

3.3.3.1 Water cooled condenser

The heat transfer rate over the WCC is calculated using the effectiveness defined in Equation 2.10-2.11 for a cross-flow heat exchange

$$\dot{Q}_{\mathrm{wcc}} = \epsilon_{\mathrm{wccCross}}\, C_{\mathrm{min}}\, (T_{\mathrm{d}} - T_{\mathrm{radClntOut}}) \tag{3.35}$$

The coolant in the WCC is the radiator outlet for cooling mode 1, but it differs depending on the mode. The outlet temperature of the saturated refrigerant vapor is however computed as

$$T_{\mathrm{wccRefOut}} = T_{\mathrm{d}} - \frac{\dot{Q}_{\mathrm{wcc}}}{\dot{m}_{\mathrm{cmpr}} c_{\mathrm{p,ref}}} \tag{3.36}$$

3.3.3.2 Air cooled condenser

The ACC supplies the vehicle cabin with hot air using the outside air to absorb heat from the refrigerant leaving the WCC. In contrast to the WCC, the refrigerant change phase during the process. The refrigerant enters the ACC as saturated vapor and condenses to a subcooled liquid. Therefore the air need to absorb the heat which condenses the refrigerant from saturated vapor to saturated liquid. The heat transfer rate which describes this process is calculated as

$$\dot{Q}_{\mathrm{accCond}} = \Delta h_{\mathrm{accCond}} \dot{m}_{\mathrm{cmpr}} \tag{3.37}$$

where ϵ is the effectiveness according to Equation 2.9 and $\Delta h_{\mathrm{accCond}}$ the latent heat condensation being the required enthalpy change in order to condense the vapor, moving across the mixed region in Figure 2.5. The remaining heat transfer which decreases the temperature of the refrigerant is

$$\dot{Q}_{\mathrm{accTemp}} = \epsilon_{\mathrm{accPhaseShift}}\, C_{\mathrm{min}}\, (T_{\mathrm{wccRefOut}} - k_{\mathrm{acc}} T_{\mathrm{ambientAir}}) \tag{3.38}$$

The temperature of the air at the ACC outlet is computed from the total enthalpy $\dot{Q}_{\mathrm{accTot}} = \dot{Q}_{\mathrm{accCond}} + \dot{Q}_{\mathrm{accTemp}}$

$$T_{\mathrm{accAirOut}} = T_{\mathrm{ambientAir}} + \frac{\dot{Q}_{\mathrm{accTot}}}{\dot{m}_{\mathrm{condAir}} c_{\mathrm{p,air}}} \tag{3.39}$$

Whereas the decreased refrigerant temperature at the outlet is a fraction of the total heat transferred

$$T_{\mathrm{accRefOut}} = T_{\mathrm{wccRefOut}} - \frac{\dot{Q}_{\mathrm{accTot}}}{\dot{m}_{\mathrm{cmpr}} c_{\mathrm{p,ref}}} \tag{3.40}$$

3.3.3.3 Validation of condensation subsystem

This section presents the result of the ACC and WCC for an ambient temperature of -10°C, 0°C, 40°C, and 45°C. The components of interest are the temperatures of the refrigerant at the ACC and WCC outlet.

Ambient temperature -10°C

The outlet temperatures from the condensers are presented in Figure 3.20 below. It shows that the refrigerant temperature at the WCC outlet is overestimated, whereas the ACC outlet temperature is underestimated. The incorrect temperatures are either caused by an incorrect mass flow rate or an estimation of the effectiveness of the NTU method.

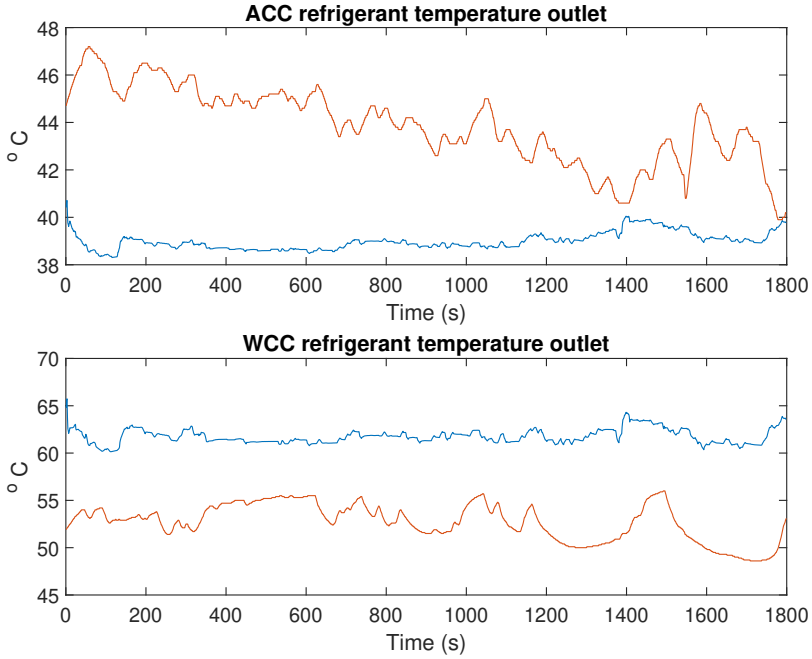

Figure 3.20: Output from the condenser of the isolated refrigerant subsystem with ambient temperature -10°C. The red line corresponds to the measurement and the blue line is the model estimation.

Ambient temperature 0°C

The model has difficulties estimating the cyclic behavior at the condenser outlets, which is presented in Figure 3.21. The estimation of ΔP deviates from the measured pressure difference since the map of the mass flow rate is limited. It causes the estimated refrigerant temperature at the compressor outlet to be noisy as well. The outlet temperature impacts the WCC which in turn affects the heat transfer rate in the ACC.

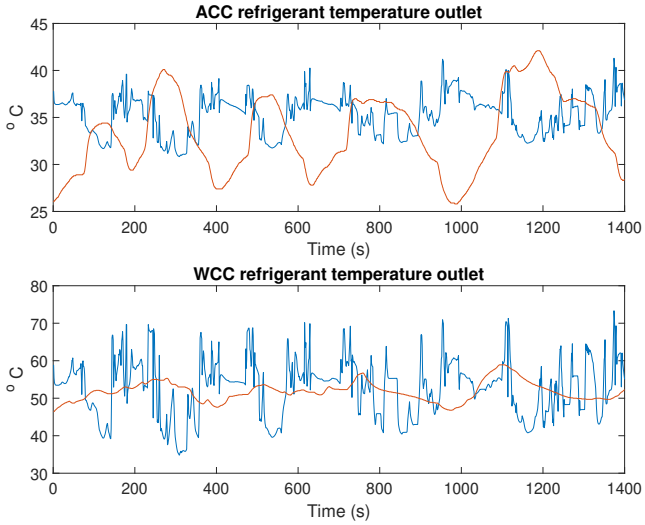

Figure 3.21: Output from the condenser of the isolated refrigerant subsystem with ambient temperature 0°C. The red line corresponds to the measurement and the blue line is the model estimation.

Ambient temperature 40°C

Both the temperature at the ACC and WCC outlet follows the trend well, but are constantly some degrees below their corresponding measurement. The deviation can for instance be caused by an incorrect effectiveness, mass flow rate, or ΔP. Figure 3.18 show that the pressure is underestimated which could cause the inlet refrigerant temperature to deviate.

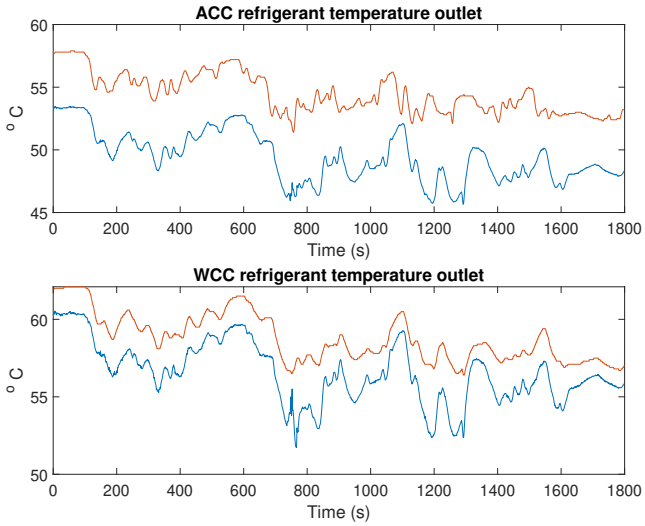

Figure 3.22: Output from the condenser of the isolated refrigerant subsystem with ambient temperature 40°C. The red line corresponds to the measurement and the blue line is the model estimation.

Ambient temperature 45°C

Like the case with an ambient temperature 40°C, the model is able to estimate the temperatures at the outlet of the ACC and WCC well. It captures even the fast dynamics as seen in Figure 3.23.

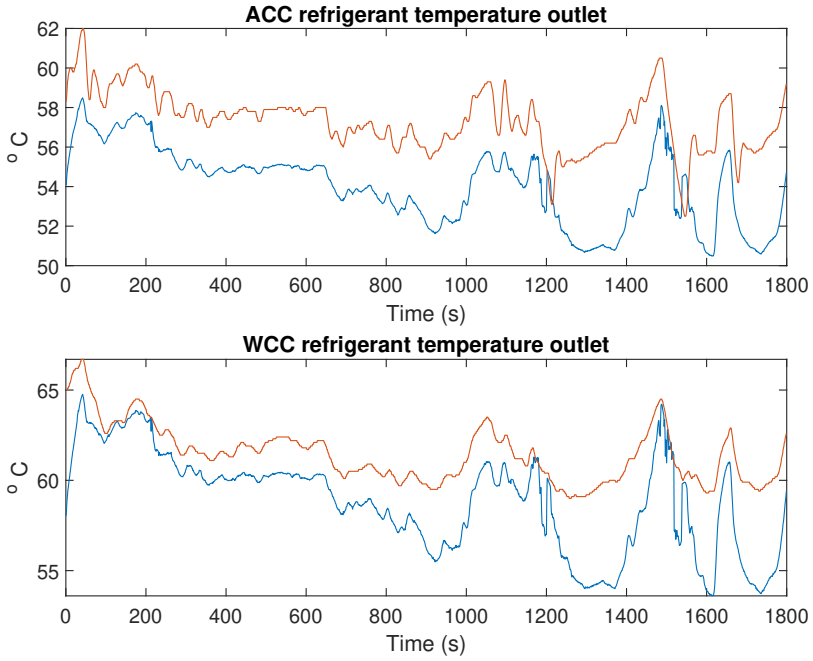

Figure 3.23: Output from the condenser of the isolated refrigerant subsystem with ambient temperature 45°C. The red line corresponds to the measurement and the blue line is the model estimation.

Table 3.7 shows the RMS error of the ACC and WCC. The model is able to capture the fast dynamics in 40°C and 45°C which yields the smallest error of the condenser.

Table 3.7: RMS error for the condenser of the isolated refrigerant subsystem

RMSE / Signal	-10	0	40	45
$\mathbf{T_{accRefOut}}$	5.0288	16.4151	5.1677	3.4663
$\mathbf{T_{wccRefOut}}$	9.9779	23.9869	2.3657	3.0429

3.4 Cabin

One of the main objectives of a vehicle's climate system is to maintain a comfortable temperature in the passenger cabin. This is controlled by the heated and cooled air from the ACC and evaporator and how these air flows are either wasted from the system or blown into the cabin. The temperature and the mass flow of the two air flows are modeled in Section 3.3.1 and 3.3.3.2 and the temperature of the air blown

into the cabin is modeled as

$$T_{\text{HVAC}} = \frac{(b_{\text{hot}}\dot{m}_{\text{accAir}}T_{\text{accAirOut}} + b_{\text{cold}}\dot{m}_{\text{evapAir}}T_{\text{evapAirOut}})}{b_{\text{hot}}\dot{m}_{\text{accAir}} + b_{\text{cold}}\dot{m}_{\text{evapAir}}} \tag{3.41}$$

The mass flow rate of air into the cabin depends on the air flows over the ACC and evaporator, which is formulated as

$$\dot{m}_{\text{HVAC}} = d_{\text{hot}}\dot{m}_{\text{accAir}} + d_{\text{cold}}\dot{m}_{\text{evapAir}} \tag{3.42}$$

The heat exchange between the air flowing into the cabin and the air inside it is modeled as

$$\dot{Q}_{\text{HVAC}} = \dot{m}_{\text{HVAC}}c_{\text{p,air}}(T_{\text{cabinAir}} - T_{\text{HVAC}}) \tag{3.43}$$

Apart from the air conditioning, there is also heat generated inside the cabin as the passengers exchange heat with the cabin air having the notation $\dot{Q}_{\text{pass}}$ [15]. The temperature of the cabin is updated as

$$T_{\text{cabinAir}} = T_{\text{cabinAir}} + \frac{\dot{Q}_{\text{pass}} - \dot{Q}_{\text{HVAC}}}{\rho_{\text{air}}c_{\text{p,air}}V_{\text{cabin}}} \tag{3.44}$$

with V_{cabin} being the cabin volume, ρ_{air} the density of air and $c_{\text{p,air}}$ its specific heat capacity.

The air mass flow over the evaporator and ACC is estimated based on the speed of the fan placed in front of the component, as illustrated in Figure 2.1. As described in Section 2.4.1 the test car suffers from air leakage. Where the leakage of ambient air depends on the recirculation door and the velocity of the car. The temperature of the air in the cabin is therefore modified as

$$T_{\text{cabinAir}} = T_{\text{cabinAir}} + \frac{\dot{Q}_{\text{pass}} - \dot{Q}_{\text{HVAC}}}{\rho_{\text{air}}c_{\text{p,air}}V_{\text{cabin}}} + b_{\text{rec}}T_{\text{ambientAir}}x_2\text{v}^2 \tag{3.45}$$

where b_{rec} is the position of the recirculation door and x_2 is a correction factor to compensate the velocity dependency.

3.4.1 Validation of the cabin

This section presents the result of the cabin temperature for an ambient temperature of -10°C, 0°C, 40°C, and 45°C.

Ambient temperature -10°C

The temperature in the passenger cabin with an ambient temperature of -10°C is presented in Figure 3.24. The estimated temperature follows the trend in the measurement but is too low.

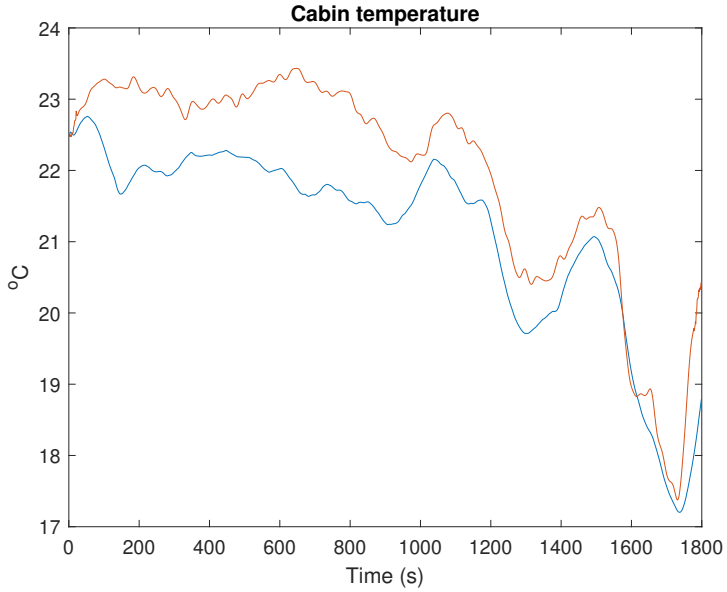

Figure 3.24: Output from the cabin of the isolated refrigerant subsystem with ambient temperature -10°C. The red line corresponds to the measurement and the blue line is the model estimation.

Ambient temperature 0°C

The cabin temperature in Figure 3.25 shows an exaggerated cyclic behavior compared with the measured temperature. The average temperature is however captured by the model.

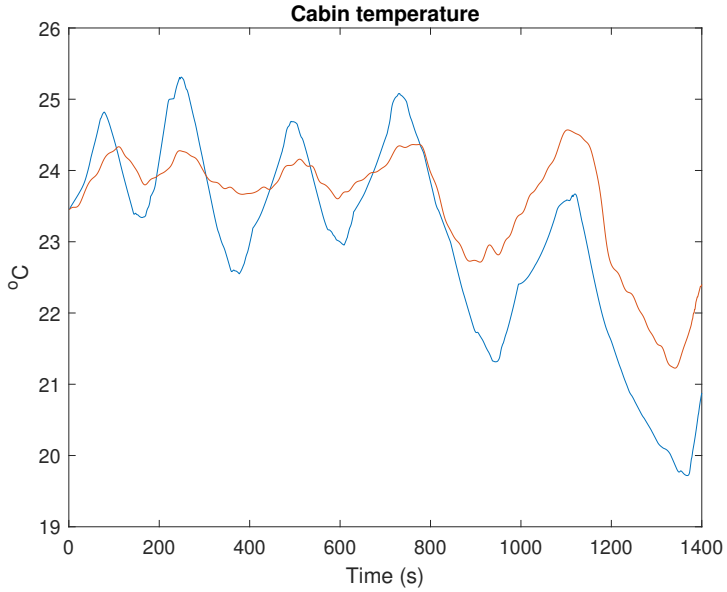

Figure 3.25: Output from the cabin of the isolated refrigerant subsystem with ambient temperature 0°C

Ambient temperature 40°C

As the velocity of the car enters the extra high speed section of the WLTP the cabin temperature becomes overestimated as seen in Figure 3.26. The recirculation door regulates the proportion of air over the evaporator that comes from the cabin respectively the outside air. Initially, the door is open and the majority of air comes from the cabin, but after approximately 1100 seconds it closes. It is likely that the leakage increases the more the door is closed, as more air is taken from the outside. On the other hand, if the door is fully open the leakage of ambient air is minimal. Therefore the cabin temperature is underestimated in the beginning as barely any additional ambient air is leaking into the evaporator. But, when the recirculation door closes the cabin temperature becomes overestimated. How the cabin model is adjusted to account for the leakage and velocity dependency is further discussed in Section 2.4.1.

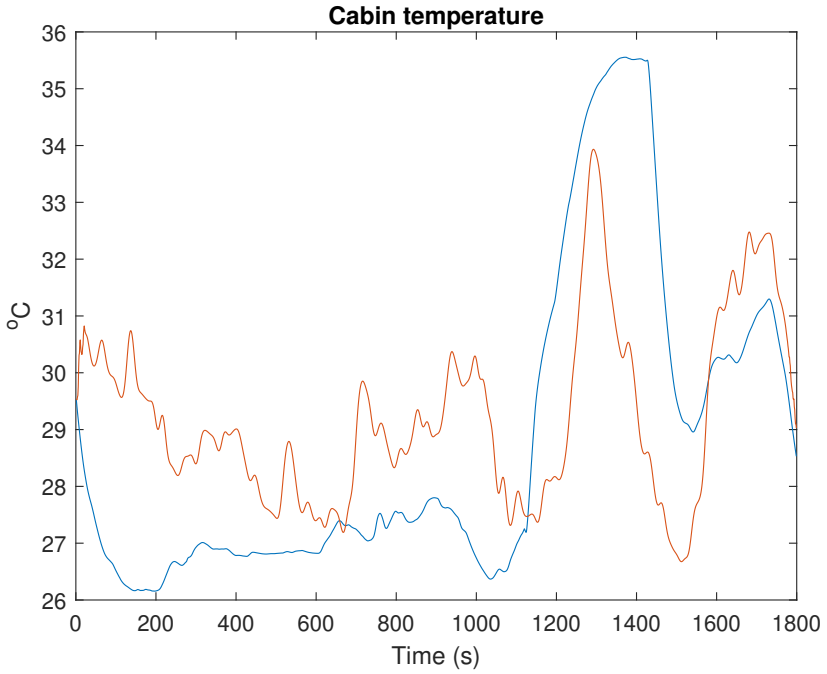

Figure 3.26: Output from the cabin of the isolated refrigerant subsystem with ambient temperature 40°C. The red line corresponds to the measurement and the blue line is the model estimation.

Ambient temperature 45°C

In contrast to the previous case with an ambient temperature of 40°C, the recirculation door is 95 per cent open throughout this driving cycle. The estimated cabin temperature is therefore too low as the mass flow of air over the evaporator is underestimated. The leakage of ambient air leads to an increased mass flow rate of air but also increases the temperature of the air over the evaporator. The 45°C outside air is significantly warmer than the cabin air which is about 30°C.

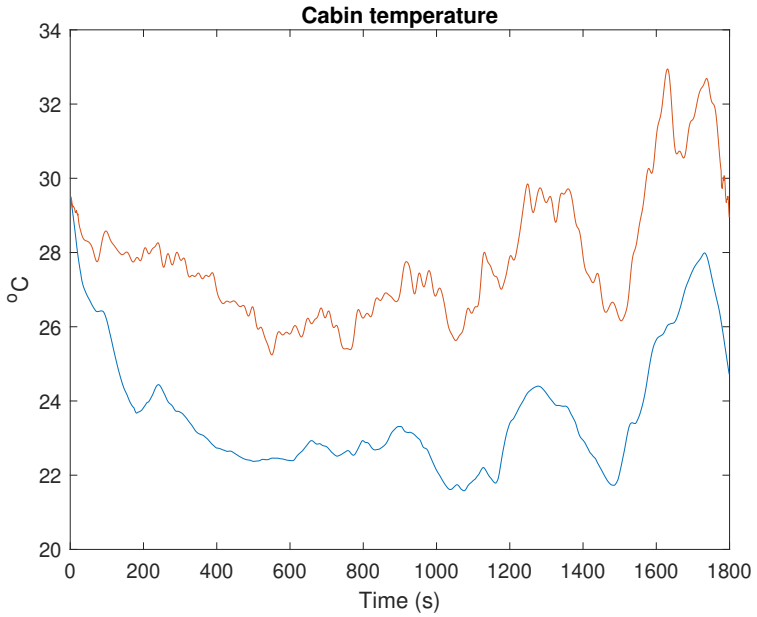

Figure 3.27: Output from the cabin of the isolated refrigerant subsystem with ambient temperature 45°C. The red line corresponds to the measurement and the blue line is the model estimation.

The RMS error of the cabin temperature is listed in Table 3.8 below

Table 3.8: RMS error for the cabin of the isolated refrigerant subsystem

RMSE / Signal	-10	0	40	45
$\mathbf{T_{cabin}}$	0.9417	0.7876	2.9715	4.2483

3.5 Simulation method

One of the main purposes of the model is to achieve a faster simulation run-time, the simulation time step is set high to one second. A large step requires fewer calculations to complete the cycle with the trade-off in accuracy as the model has a fixed behavior for one time step. In a non-linear system, a too large time step can cause the model to make exaggerated changes and not represent fast model dynamics with a simple method such as the linear Euler method. An alternative is the Runge-Kutta method which is also a one step method where several points are used to estimate the solution [16]. By using multiple points the solution will be more numerically stable. With the fourth order of Runge-Kutta, the solution is calculated as

$$k_1 = \Delta t f(t_i, y_i) \tag{3.46}$$

$$k_2 = \Delta t f(t_i + \frac{1}{2}\Delta t, y_i + \frac{1}{2}k_1) \tag{3.47}$$

$$k_3 = \Delta t f(t_i + \frac{1}{2}\Delta t, y_i + \frac{1}{2}k_2) \tag{3.48}$$

$$k_4 = \Delta t f(t_i + \Delta t, y_i + k_3) \tag{3.49}$$

$$y_{i+1} = y_i + \frac{1}{6}(k_1 + k_2 + k_3 + k_4) \tag{3.50}$$

4

Results

This chapter presents the result of the complete thermal model, described in Section 2.1, along with the RMS error of the outputs for each ambient temperature.

4.1 Model validation

The complete model is evaluated by connecting the coolant and the refrigerant systems described in Section 3.2 and 3.3, with the model estimating all system states given the initial values and the control signals. The signals of interest are the outputs listed in Table 3.1 together with control signals of EXV openings, and the compressor speed. The refrigerant mass flow is included to explain the model behavior. With the two subsystems being connected the errors from the isolated circuits can now expand across the system.

4.1.1 Ambient temperature -10°C

As seen in the isolated subsystems in Sections 3.2 and 3.3 the models were able to follow the reference with small deviations. The battery and cabin temperature presented in Figure 4.1 shows a small deviation for the outputs. Along with the battery state of charge (SoC) which also has a small deviation.

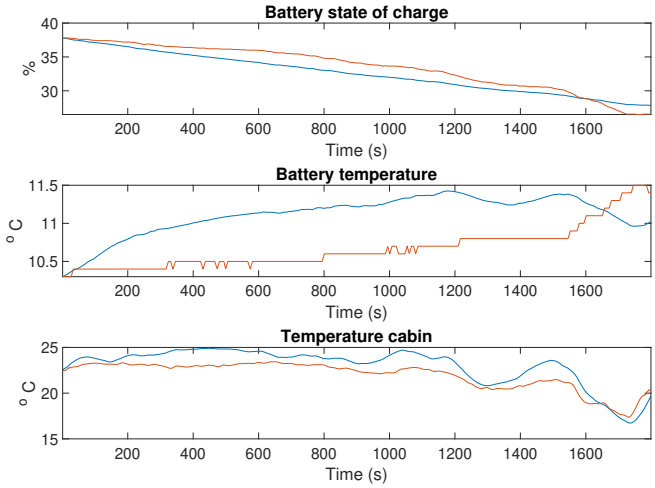

Figure 4.1: Battery output of the complete plant model with ambient temperature -10°C. The red line corresponds to the measurement and the blue line is the model estimation.

The error in the coolant model seen in Section 3.2 affects the refrigerant subsystems with the lower coolant temperature decreasing the temperature of the refrigerant suction temperature at the final third of the cycle. This is seen in Figure 4.2 with the lower chiller coolant temperature meaning a smaller heat exchange, resulting in the lower refrigerant temperature seen in Figure 4.3.

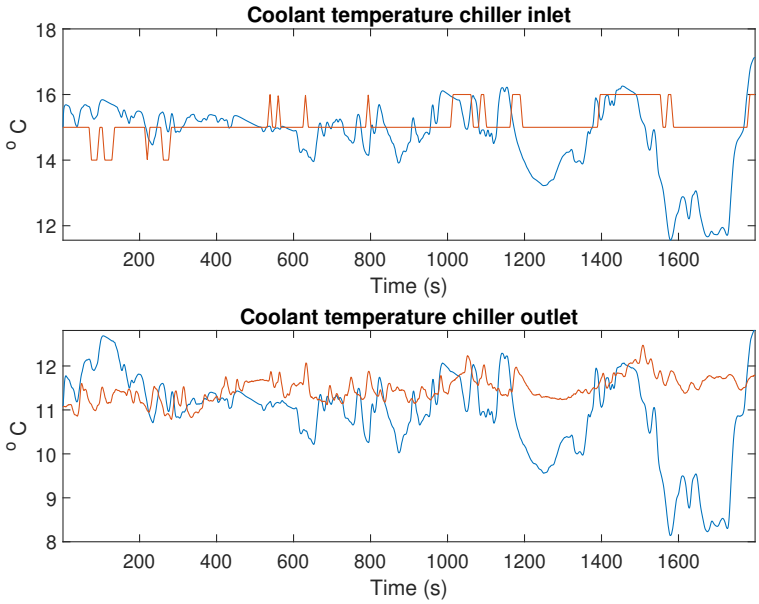

Figure 4.2: Chiller output of the complete plant model with ambient temperature -10°C. The red line corresponds to the measurement and the blue line is the model estimation.

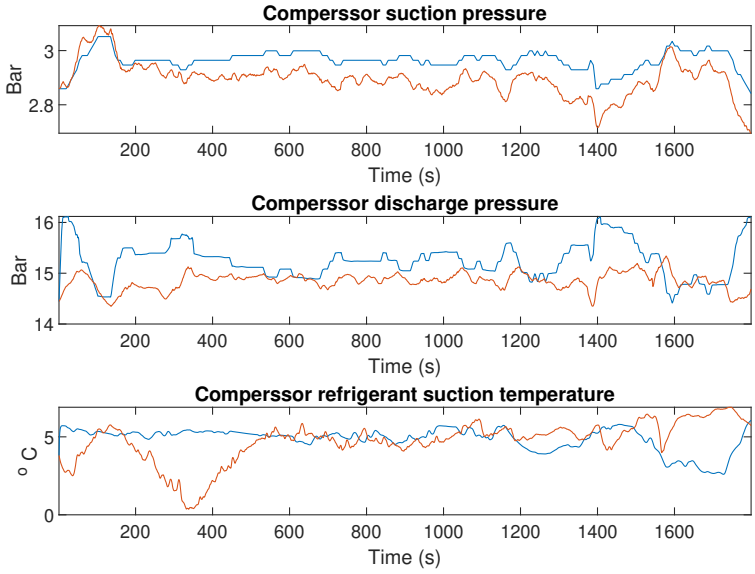

Figure 4.3: Compressor output of the complete plant model with ambient temperature -10°C. The red line corresponds to the measurement and the blue line is the model estimation.

The model errors for the cold scenario of -10°C can be seen in Table 4.1 with minor deviations that shift the systems equilibrium point. The system has a steady behavior with small changes in the control signals seen in Figure 4.4 with the model being able to follow the system behavior.

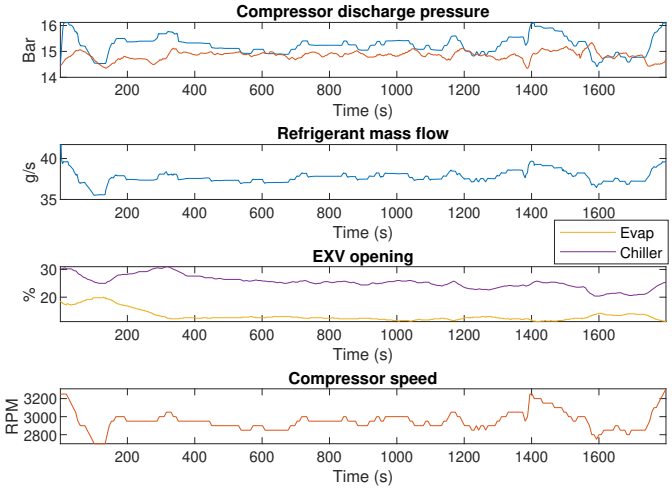

Figure 4.4: Control signals used to estimate the complete plant model with ambient temperature -10°C. The red line corresponds to the measurement and the blue line is the model estimation.

4.1.2 Ambient temperature 0°C

The periodic behavior in the chiller EXV opening and the compressor speed seen in Figure 4.8 causes the complete system to follow that pattern having the temperatures differ from the physical system. With the battery coolant pump switched off as described in Section 3.2.2.1, the battery shown in Figure 4.5 is not affected by this. Chiller coolant deviates as seen in Figure 4.6 with an explanation in Section 3.2.2.1.

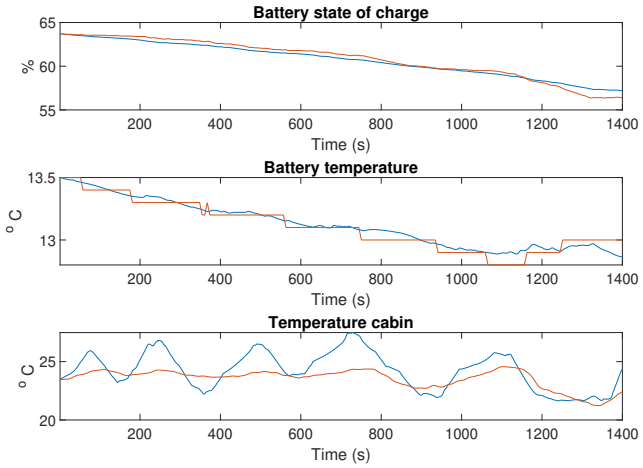

Figure 4.5: The battery output of the complete plant model with ambient temperature 0°C. The red line corresponds to the measurement and the blue line is the model estimation.

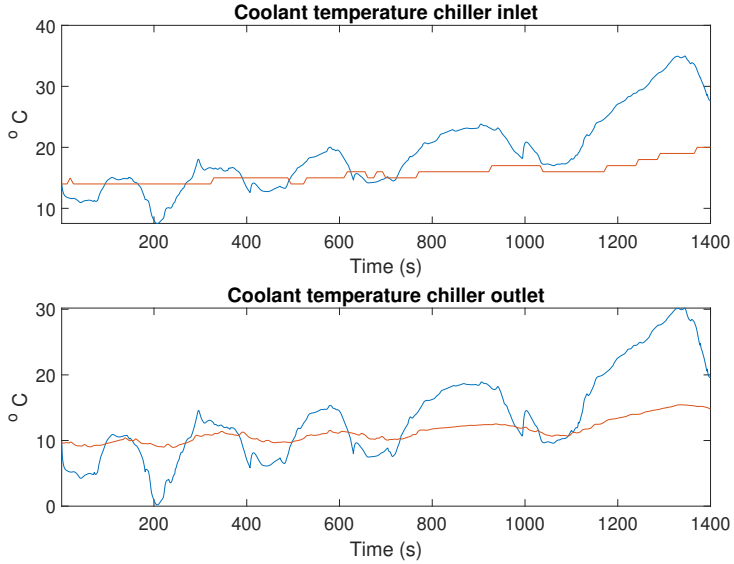

Figure 4.6: The chiller output of the complete plant model with ambient temperature 0°C. The red line corresponds to the measurement and the blue line is the model estimation.

The issue is introduced to the system with the refrigerant mass flow being incorrect.

With the mass flow being mapped from a limited set of data points with gaps in the points, interpolated values get affected to be inaccurate. The suction pressure is close to its reference while the discharge is not, confirming that the refrigerant mass flow is inaccurate since the discharge pressure is updated with ΔP which is based on the mass flow and can be seen in Figure 4.7.

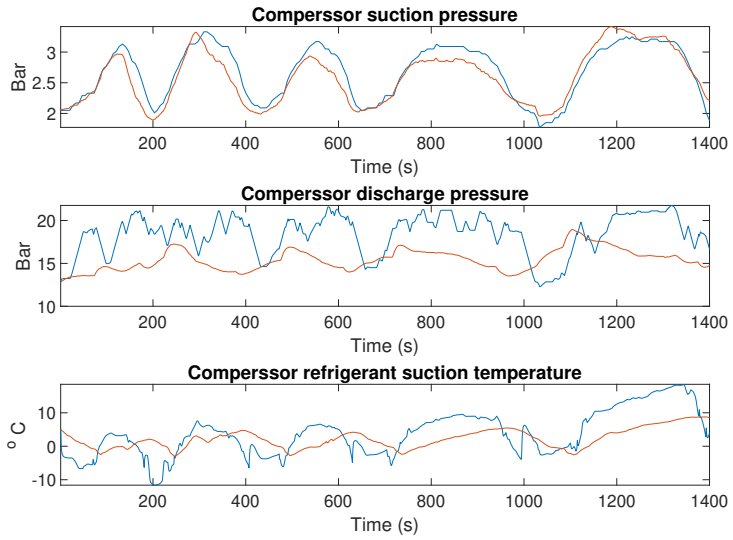

Figure 4.7: The compressor output of the complete plant model with ambient temperature 0°C. The red line corresponds to the measurement and the blue line is the model estimation.

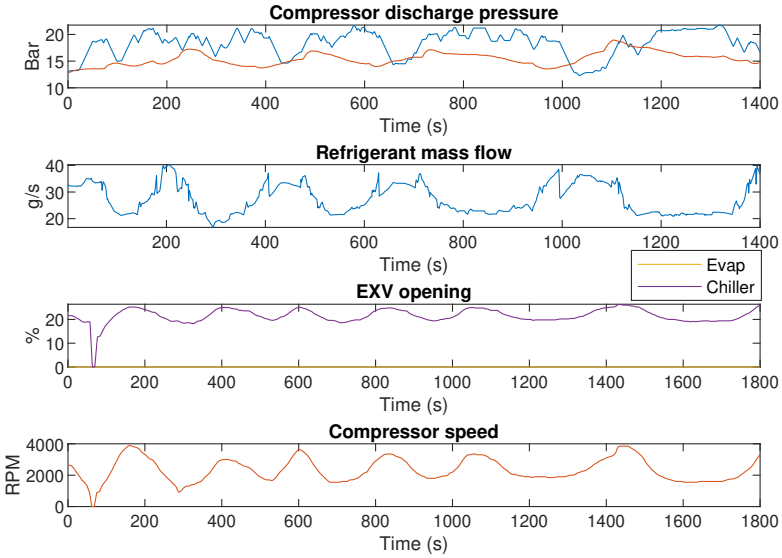

Figure 4.8: Control signals used to estimate the complete plant model with ambient temperature 0°C. The red line corresponds to the measurement and the blue line is the model estimation.

4.1.3 Ambient temperature 40°C

The chiller EXV is closed for the entire cycle which can be seen in Figure 4.12 meaning that there is no exchange between the battery circuit and the refrigerant, Figure 4.5-4.10 shows the battery and chiller coolant having the same result as the isolated case.

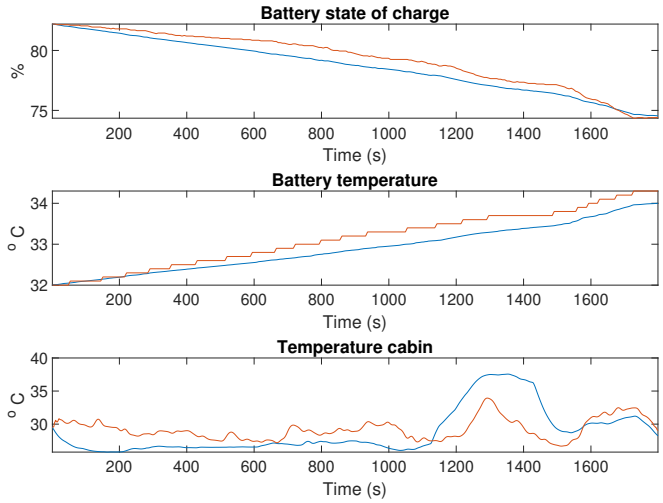

Figure 4.9: The battery output of the complete plant model with ambient temperature 40°C. The red line corresponds to the measurement and the blue line is the model estimation.

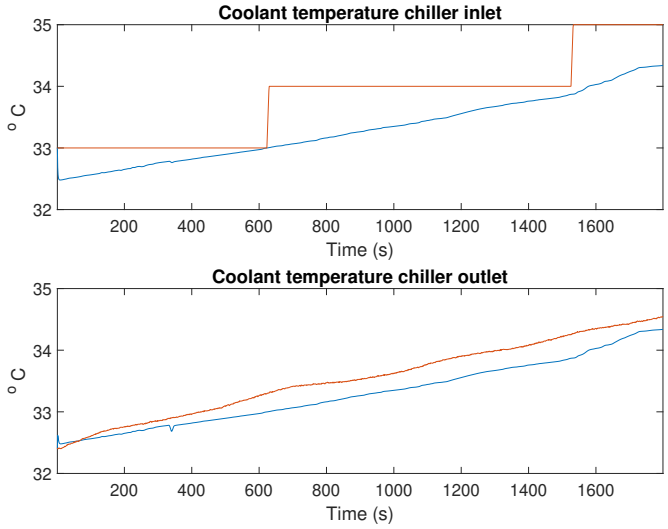

Figure 4.10: The chiller output of the complete plant model with ambient temperature 40°C. The red line corresponds to the measurement and the blue line is the model estimation.

The compressor pressure and temperature follow the reference with small errors where a short drop in the compressor speed is seen in Figure 4.12, causing the drop

in discharge pressure illustrated in Figure 4.11.

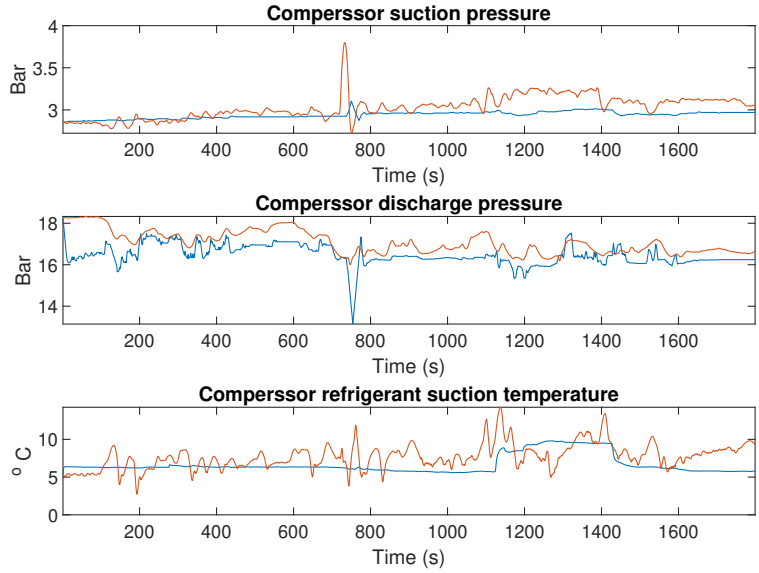

Figure 4.11: The compressor output of the complete plant model with ambient temperature 40°C. The red line corresponds to the measurement and the blue line is the model estimation.

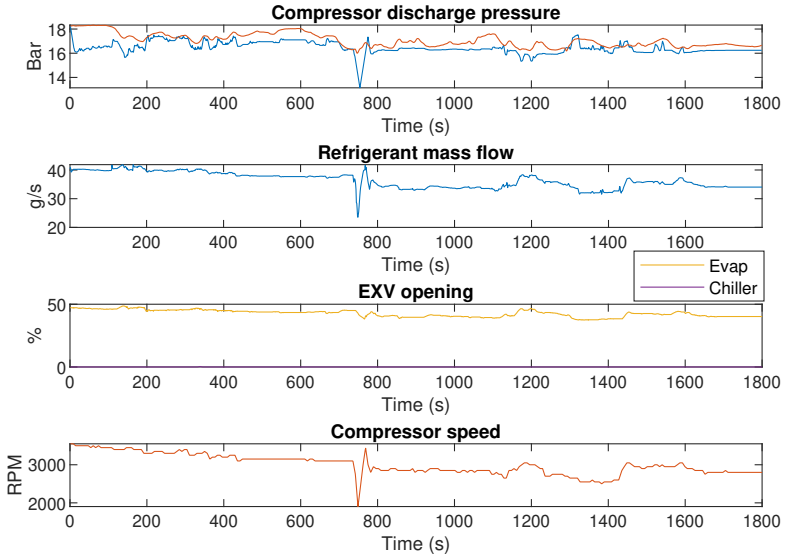

Figure 4.12: Control signals used to estimate the complete plant model with ambient temperature 40°C. The red line corresponds to the measurement and the blue line is the model estimation.

4.1.4 Ambient temperature 45°C

Just as for 40°C the chiller EXV is closed for the majority of the cycle shown in Figure 4.16 and the chiller coolant and battery is tracking the references seen in Figures 4.13-4.14 just as the isolated case.

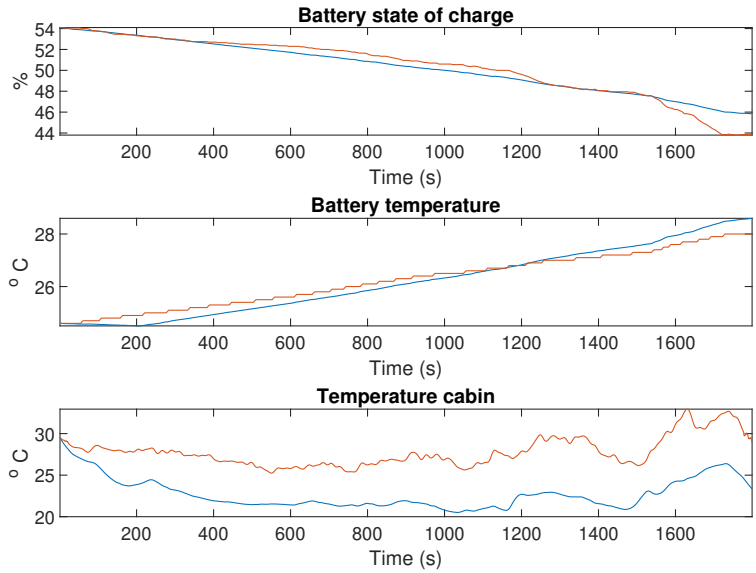

Figure 4.13: The battery output of the complete plant model with ambient temperature 45°C. The red line corresponds to the measurement and the blue line is the model estimation.

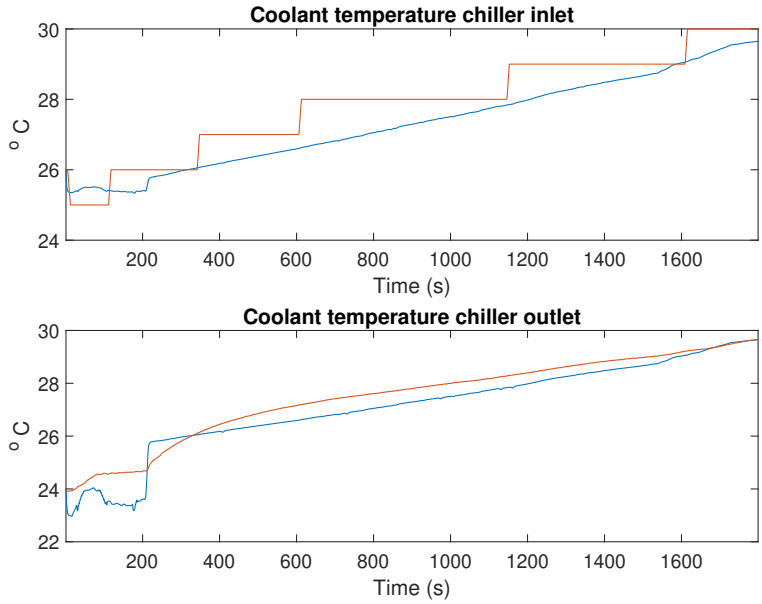

Figure 4.14: The chiller output of the complete plant model with ambient temperature 45°C. The red line corresponds to the measurement and the blue line is the model estimation.

In the initial phase of the cycle it can be seen in Figure 4.15 that the discharge pressure has an offset which is during the same period as both EXVs are open. This indicates that the modeling of the EXVs with a small opening is non-accurate. The control signal for the evaporator EXV increases the same amount as the chiller EXV decreases around time step 200. After that moment the discharge pressure becomes closer to the reference again.

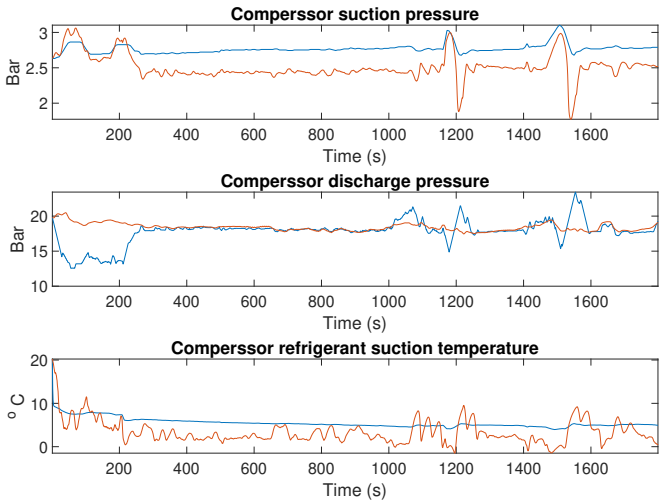

Figure 4.15: The compressor output of the complete plant model with ambient temperature 45°C. The red line corresponds to the measurement and the blue line is the model estimation.

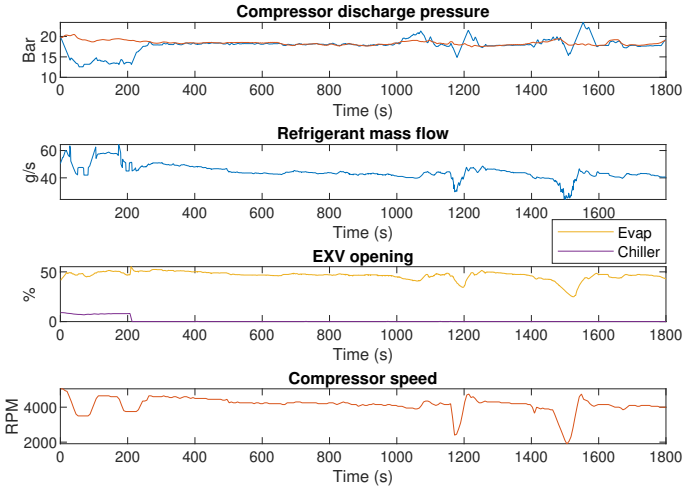

Figure 4.16: Control signals used to estimate the complete plant model with ambient temperature 45°C. The red line corresponds to the measurement and the blue line is the model estimation.

Table 4.1: RMS error for the complete model

RMSE / Signal	-10	0	40	45
SoC	0.9417	0.0042	0.0072	0.0071
$\mathbf{T_{batt}}$	0.0129	0.0487	0.2709	0.2808
$\mathbf{T_{cabin}}$	0.4932	0.5439	2.9714	4.2482
$\mathbf{P_s}$	1.0669	0.1934	0.1477	0.2959
$\mathbf{T_s}$	0.0794	7.9331	1.9630	3.0788
$\mathbf{P_d}$	1.7887	3.9151	0.7783	2.1097
$\mathbf{T_{chillIn}}$	1.1238	5.9818	0.5789	0.6806
$\mathbf{T_{chillOut}}$	1.1514	5.6914	0.2665	0.5117

5
Conclusion

This chapter summarized the model performance presented in the previous chapter with the simulation results discussed. Conclusions based on the model results and what causes its errors is presented.

In accordance with the aim of this thesis, a plant of the TEM system was designed and it manages to simulate the behavior of the physical car. As further stated in the thesis aim, the model simulates the system with a fast run-time and is able to represent the system for a large range of temperatures.

As formulated in Chapter 1, the main focus of contribution was to design a model of the system that remains representative of minor offsets for its complete usage range of ambient conditions. Result figures from the simulations presented in Chapter 3 show that the model of individual subsystems is capable to follow the desired behavior of the reference and is able to do so for all evaluated temperatures. As the coolant circuit does not involve any phase shifts it is less complex which is highlighted in the RMS error in relation to the refrigerant circuit. The refrigerant circuit encounters multiple phase shifts at different pressures adding to its complexity. As illustrated in Figure 3.12 and 3.23 and showed in Table 3.5 and 3.7 the refrigerant circuit has larger offsets and more dynamic behavior. However, the model remains stable, following the same pattern with a shifted system equilibrium point.

There are multiple factors combined causing the errors to develop in the form of model deviations, with contributions from modeling simplifications, limited access to data, and inconsistent measurement data. The model simplifications explained in Section 3.1 are all added to a less accurate model, although certain assumptions have more influence on the system's overall performance than others. The presumption that the two expansion valves are considered as one when estimating the pressure difference between the high and low side shows varying results. Both valves are simultaneously open for the complete cycle at -10°C with a good model output seen in Figure 4.4. The opposite can be seen at 40°C in Figure 4.12 when the two valves are initially open, the pressure difference is inaccurate but the model manages to recover once the chiller EXV closes without remaining disturbances in the simulation model.

Another focus area was the heat transfer over the evaporator and ACC where the major part of energy was consumed to change the refrigerant phase. As described in Section 2.4 the air mass flows over the evaporator and ACC are inaccurately estimated by the system with leakage from ambient air. Calculating the heat transfer using the indicated mass flow by the system resulted in a far too small $\dot{Q}$ such that the refrigerant would not be vaporized. This highlights how the mass flows are

incorrect and their values unreliable, making it difficult to know what levels to trust with the air flows being in focus since that in contrast to the coolant and refrigerant flows are not sealed from external impact. It is important to keep in mind that the vehicle is a prototype under development with the next build series bringing improvements to the hardware. This will likely influence the behavior of the vehicle such that the current model is no longer representative of the physical product. The base of the model however still represents the expected behavior of the system with adaptations to the flaws of the test car as described in Section 2.4. With new measurements, the model can quickly be adjusted to an updated system.

The validation of the separated subsystems in Section 3.2-3.4 showed the model had the desired behavior with varying deviations in an acceptable range. With the subsystems coupled together in Chapter 4 the figures illustrated that these errors spread across the system to slightly increase the errors. However, the model manages to find a new equilibrium point to operate at with a stable behavior that still captures the dynamics of the system as seen in Figure 4.1-4.16. This confirms the model to have the ability to simulate the TEM system to be represented in a reliable way. In addition, the model is independent of system data such that it can be utilized as a verification tool of the control software.

6
Future work

This chapter presents further improvements to the plant model. Based on the result and drawn conclusions three fields of further work are presented. It contains machine learning to reduce the deviation between the analytical plant model and the physical system, further verification of the model, and additional sensors to improve the measured signals.

Reduced model error using machine learning

The plant model of the thermal system could be improved further by decreasing the model error using machine learning. As discussed previously, the model has difficulties adapting to fast dynamic changes leading to nonreactive behavior. Based on test data a machine learning part could learn the existing model error in each time step. The plant model could then be updated such that it better represents the rapid changes in the thermal system in the physical car. Using machine learning however requires an extensive amount of data to train on, which is a limiting factor. Moreover, machine learning could also be used to model complex parts of the refrigerant circuit such as the estimated mass flow over two expansion valves in parallel. Further research could be done on circuits with several valves and how to determine its mass flow coefficient correctly.

Verification on additional scenarios

The model is adapted to manage changes in coolant mode within a driving cycle, but the measurement data used do not contain mode shifts. Furthermore, the measurement data is collected in a steady state which means that the model is not tested on corner cases. For instance, a startup sequence when the battery is not already cooled when the ambient temperature is 45 degrees. To verify that the plant model represents the physical system well it is of interest to test it on different data additional to the WLTP.

Improved measurements

Another field of improvement is adding sensors to determine the accuracy of the estimated mass flows. The software estimates the mass flow rate of air over the ACC and evaporator based on the corresponding fan speed. But it has been shown that the estimations are inaccurate. Adding sensors that measure the air mass flow would give further knowledge of the accuracy of the software estimations. Also

measuring the refrigerant mass flow would give an insight into the limitations of the compressor map since it has shown that the map has a limited number of data points. The collected measurements from the WLTP are generally treated as the ground truth of the thermal system. Taking the measurement uncertainty into consideration would also improve the plant model further.

Bibliography

[1] N. Rietmann, B. Hügler, and T. Lieven, "Forecasting the trajectory of electric vehicle sales and the consequences for worldwide co2 emissions", vol. 261, 2020. DOI: 10.1016/j.jclepro.2020.121038.

[2] M. Jeffers, L. Chaney, and J. Rugh, "Climate control load reduction strategies for electric drive vehicles in warm weather", vol. 1, Apr. 2015. DOI: 10.4271/2015-01-0355.

[3] P. Lokur, K. Nicklasson, L. Verde, M. Larsson, and N. Murgovski, "Modeling of the thermal energy management system for battery electric vehicles", *2022 IEEE Vehicle Power and Propulsion Conference (VPPC)*, vol. 27, no. 2, pp. 1–7, 2023.

[4] V. C. Agency. "The worldwide harmonised light vehicle test procedure (wltp)". (Apr. 2021), [Online]. Available: https://www.vehicle-certification-agency.gov.uk/fuel-consumption-co2/the-worldwide-harmonised-light-vehicle-test-procedure/. (accessed: 14.05.2023).

[5] R. Chhabra, *CRC Handbook of Thermal Engineering*. Taylor Francis, 2018.

[6] D. I. K. M, *REFRIGERATION SYSTEMS AND APPLICATIONS*. John Wiley Sons, 2012.

[7] MEP Academy instructor. "How electronic expansion valves work", MEP Academy. (Jan. 2022), [Online]. Available: https://mepacademy.com/how-electronic-expansion-valves-work/. (accessed: 03.03.2023).

[8] C. Liu, J. Zhang, Y. Gui, *et al.*, "Mass flow characteristics and empirical modeling of r744 flow through electronic expansion device", *International Journal of Refrigeration*, vol. 86, pp. 82–88, 2018.

[9] W. Li, "Simplified modeling analysis of mass flow characteristics in electronic expansion valve", vol. 53, Apr. 2013. DOI: 10.1016/2012-12-035.

[10] P. Von Böckh and T. Wetzel, *Heat Transfer Basic and Practise*. Springer, 2012.

[11] J. Lienhard IV and J. Lienhard V, *A Heat Transfer Textbook*. Phlogiston Press, 2020.

[12] W. Roetzel, X. Luo, and D. Chen, *Design and operation of heat exchangers and their networks*. Academic Press, 2019.

[13] G. Liu, M. Ouyang, L. Lu, J. Li, and X. Han, "Analysis of the heat generation of lithium-ion battery during charging and discharging considering different influencing factors", *Journal of Thermal Analysis and Calorimetry*, vol. 116, pp. 1001–1010, 2014.

[14] C. Wadhwa, *Electrical power systems*. New Age International, 2006.

[15] X. Zhou, D. Lai, and Q. Chen, "Experimental investigation of thermal comfort in a passenger car under driving conditions", *Building and environment*, vol. 149, pp. 109–119, 2019.

[16] M. Koga, N. Tanimura, and T. Sato, "Numerical simulation using runge-kutta method for the system with uncertain discontinuous change", in *Proceedings of the 41st SICE Annual Conference. SICE 2002.*, IEEE, vol. 5, 2002, pp. 2749–2753.

DEPARTMENT OF SOME SUBJECT OR TECHNOLOGY
CHALMERS UNIVERSITY OF TECHNOLOGY
Gothenburg, Sweden
www.chalmers.se

CHALMERS
UNIVERSITY OF TECHNOLOGY